The MNT transcription factor autoregulates its expression and supports proliferation in MYC-associated factor X (MAX)-deficient cells

Received for publication, July 28, 2019, and in revised form, December 16, 2019 Published, Papers in Press, January 9, 2020, DOI 10.1074/jbc.RA119.010389

M. Carmen Lafita-Navarro[‡1,2], Judit Liaño-Pons[‡1,3], Andrea Quintanilla[‡4], Ignacio Varela[‡], Rosa Blanco[‡], Fabiana Ourique[‡5], Gabriel Bretones[‡6], Julia Aresti[‡7], Ester Molina[‡], Patrick Carroll[§], Peter Hurlin[¶], Octavio A. Romero[‖], Montse Sanchez-Céspedes[‖8], Robert N. Eisenman[§], M. Dolores Delgado[‡], and Javier León[‡9]

From the [‡]Instituto de Biomedicina y Biotecnología de Cantabria (IBBTEC), Universidad de Cantabria-CSIC, and Department of Molecular Biology, Universidad de Cantabria, 39005 Santander, Spain, the [§]Division of Basic Sciences, Fred Hutchinson Cancer Research Center, Seattle, Washington 98109, the [¶]Shriners Hospitals for Children Research Center, and Department of Cell, Developmental and Cancer Biology, Knight Cancer Institute, Oregon Health and Science University, Portland, Oregon 97239, and the [‖]Genes and Cancer Group, Cancer Epigenetics and Biology Program (PEBC), Bellvitge Biomedical Research Institute–IDIBELL, 08908 Barcelona, Spain

Edited by Eric R. Fearon

The MAX network transcriptional repressor (MNT) is an MXD family transcription factor of the basic helix-loop-helix (bHLH) family. MNT dimerizes with another transcriptional regulator, MYC-associated factor X (MAX), and down-regulates genes by binding to E-boxes. MAX also dimerizes with MYC, an oncogenic bHLH transcription factor. Upon E-box binding, the MYC–MAX dimer activates gene expression. MNT also binds to the MAX dimerization protein MLX (MLX), and MNT–MLX and MNT–MAX dimers co-exist. However, all MNT functions have been attributed to MNT–MAX dimers, and no functions of the MNT–MLX dimer have been described. MNT's biological role has been linked to its function as a *MYC* oncogene modulator, but little is known about its regulation. We show here that MNT localizes to the nucleus of MAX-expressing cells and that MNT–MAX dimers bind and repress the *MNT* promoter, an effect that depends on one of the two E-boxes on this promoter. In MAX-deficient cells, MNT was overexpressed and redistributed to the cytoplasm. Interestingly, MNT was required for cell proliferation even in the absence of MAX. We show that in MAX-deficient cells, MNT binds to MLX, but also forms homodimers. RNA-sequencing experiments revealed that MNT regulates the expression of several genes even in the absence of MAX, with many of these genes being involved in cell cycle regulation and DNA repair. Of note, MNT–MNT homodimers regulated the transcription of some genes involved in cell proliferation. The tight regulation of MNT and its functionality even without MAX suggest a major role for MNT in cell proliferation.

This work was supported by Grant SAF2017-88026-R from Agencia Estatal de Investigación, Spanish Government (to J. L. and M. D. D.), funded in part by FEDER Program from the European Union, National Institutes of Health Grant CA57138/CA from NCI (to R. N. E.), and grants from Shriners Hospitals for Children (to P. J. H.). The authors declare that they have no conflicts of interest with the contents of this article. The content is solely the responsibility of the authors and does not necessarily represent the official views of the National Institutes of Health.

The RNA-seq and ChIP-seq data have been deposited to the European Nucleotide Archive with the accession number PRJEB23604.

This article contains Figs. S1–S9 and Tables S1–S8.

[1] Both authors contributed equally to this work.

[2] Recipient of an F.P.U. fellowship from the Spanish Government. Present address: Sorrell Lab, Dept. of Cell Biology, UT Southwestern Medical Center, Dallas, TX 75390.

[3] Recipient of an F.P.U. fellowship from the Spanish Government.

[4] Present address: Edinburgh Cancer Research UK Centre, Institute of Genetics and Molecular Medicine, University of Edinburgh, EH4 2XU Scotland, United Kingdom.

[5] Present address: Dept. of Biochemistry, Universidade Federal de Santa Catarina (UFSC), 88040-900 Florianópolis, Brazil.

[6] Present address: Dept. de Bioquímica y Biología Molecular, Facultad de Medicina, Instituto Universitario de Oncología (IUOPA), Universidad de Oviedo, 33003 Oviedo, Asturias, Spain.

[7] Present address: Groningen Biomolecular Sciences and Biotechnology Institute, University of Groningen, 9712 CP Groningen, Netherlands.

[8] Present address: Josep Carreras Leukemia Research Institute, Campus ICO-Germans Trias i Pujol, 08916 Badalona, Barcelona, Spain.

[9] To whom correspondence should be addressed. E-mail: leonj@unican.es.

MNT[10] is a basic helix-loop-helix leucine zipper (bHLH-LZ) protein, and it is the most divergent member of the MXD family, which also includes MXD1, MXI1, MXD3, and MXD4. MNT forms heterodimers with MAX through the bHLH-LZ domain and binds to E-box DNA sequences. MYC is one of the most prevalent human oncoproteins (1). MYC can also interact with MAX and bind E-boxes (2, 3). Whereas MYC–MAX, upon binding to E-boxes, acts primarily as a transcriptional activator, the typical effect of MNT–MAX is the transcriptional repression (4, 5). MNT can bind not only to MAX but also to the MAX-like HLH protein MLX (6, 7), which alternatively can interact with MLXIP (MONDOA) and MLXIPL (MONDOB) proteins. Therefore, MNT participates both in the MAX- and MLX-centered networks (8, 9) serving as the link between MAX–MYC and MLX–MONDO.

MNT is expressed constitutively in proliferating and quiescent cells, and the protein levels do not show major fluctuations

[10] The abbreviations used are: MNT, MAX network transcriptional repressor; bHLH-LZ, basic helix-loop-helix leucine zipper; MAX, MYC-associated factor X; qPCR, quantitative PCR; RNA-seq, RNA sequencing; FL, full-length; GSEA, Gene Set Enrichment Analysis; ChIP-seq, ChIP-sequencing; RPKM, reads per kilobase pair per million.

when quiescent cells are mitotically stimulated (5, 10, 11). *Mnt*$^{-/-}$ mice are not viable (10, 12), whereas *Mxd1*$^{-/-}$, *Mxi1*$^{-/-}$, and *Mxd3*$^{-/-}$ mice survive, suggesting that MNT function is not redundant with that of the other MXD proteins (13–15). Moreover, MNT is the only MXD-related protein in invertebrates (9).

Consistent with MNT functioning as a MYC transcriptional antagonist, enforced MNT expression inhibits cell proliferation and impairs MYC-dependent transformation (5, 11). The deficiency or down-regulation of MNT in fibroblasts leads to increased proliferation (*i.e.* similarly to MYC overexpression) and partially rescues the proliferative arrest caused by MYC deficiency (10, 11, 16, 17). MNT ablation *in vivo* leads to breast and T-cell tumors (10, 12, 17), and according to the Cancer Genome Atlas, about 10% of human tumors show deletion of a MNT allele (1).

Partial or total MNT deficiency in mouse models impairs MYC-dependent tumorigenesis (18, 19), and *MNT* knockout in some cell models inhibits proliferation and promotes apoptosis (10, 16, 17). Thus, MYC and MNT proteins co-exist in proliferating cells, and depending on the model, MNT acts as a MYC antagonist or a cooperator of MYC.

However, there is scarce information about MNT transcriptional regulation, and it is unknown whether MNT exerts functions without MAX. In this work, we studied possible MAX-independent functions of MNT using UR61 cells as the main model. These rat pheochromocytoma cells do not express a functional MAX protein but a truncated form (termed MAX^{PC12}) that lacks the second helix and leucine zipper region of the bHLH-LZ domain, which are the regions responsible for dimerization with MYC and MNT (20). Here, we describe a change of MNT subcellular localization depending on MAX expression and the repression of its own promoter in the presence of MAX. In addition, we show the first examples of MNT functions that are independent of MAX. In the absence of MAX, 1) MNT regulates gene transcription by binding to DNA through the formation of MNT–MNT or MNT–MLX complexes, and 2) MNT is required for optimal cell proliferation.

Results

MNT levels depend on MAX

To explore the effect of MAX on MNT expression, we first compared MNT and MAX levels in proliferating cells from 13 cell lines derived from different tissues and species, including two cell lines lacking MAX: UR61 and the human small-cell lung carcinoma H1417 cells (21). The results showed that although MNT expression varies among the cell lines, the two MAX-deficient cell lines and others with low MAX levels (HeLa and CEM) expressed high MNT levels, whereas other cells with high MAX levels expressed low MNT levels (293T, K562, and Ramos) (Fig. 1*A*). MNT was expressed in all cell lines as a protein doublet, due to a slower-migrating phosphorylated MNT form (22). MAX was also expressed as a doublet of 21 and 22 kDa (23). Although the correlation was not universal, the high MNT expression in some cell lines with null or low MAX levels led us to explore whether MAX influenced MNT levels.

For this purpose, we transfected UR61 cells with a construct carrying human MAX cDNA driven by the metallothionein promoter, which is activated by Zn^{2+} cations (24). Several clones were isolated, and two of them with robust MAX induction were mixed, and the resulting cells were termed URMax34. We also generated a cell line transfected with the empty vector, termed URMT, which is a pool of five transfected clones. The induction of MAX in response to Zn^{2+} in URMax34 cells was confirmed by immunoblot (Fig. 1*B*). We examined the effect of MAX induction on MNT levels in URMax34 cells, and we found that MNT was down-regulated upon MAX induction by Zn^{2+} (Fig. 1*B*). As expected, the treatment of URMT cells with Zn^{2+} did not change the MNT levels (Fig. S1*A*). To confirm this result and rule out effects potentially related to the generation of stably transfected clones (as the URMax34 system), UR61 cells were transiently transfected with a MAX expression vector, and the results showed a decrease in MNT protein levels in MAX-transfected cells (Fig. 1*C*). It is noteworthy that the down-regulation of MNT provoked by the re-expression of MAX in these cells also occurred at the mRNA levels, as determined by RT-qPCR (Fig. 1*D*). We then analyzed the effect of MAX-enforced expression in three human small-cell lung cancer cell lines deficient in MAX (21). MAX-enforced expression was achieved by lentiviral transduction, and the levels of MNT were examined by immunoblot in Lu134, Lu165, and H1417 cell lines (Fig. 1*E*). In all cell lines, MAX expression resulted in lower MNT protein levels. The MNT mRNA levels were also down-regulated in Lu165 and in H1417 cells upon MAX expression (Fig. 1*F*).

We next sought to confirm this in a different cell type with endogenous MAX. A MAX expression vector was transfected into human myeloid leukemia K562 cells. The immunoblot results showed lower MNT levels in the cells with MAX overexpression (Fig. 1*G*). Next, we used the Kmax12 cell line (24), a K562 derivative carrying a MAX transgene in which expression is induced by Zn^{2+}. Induction of MAX expression in Kmax12 cells resulted in a concomitant MNT down-regulation (Fig. 1*H*). We also used the opposite approach, *i.e.* depleting cells of MAX and analyzing the expression of MNT. As shown in Fig. 1*I*, MNT protein expression was up-regulated when MAX was silenced with siRNA in K562. Interestingly, MNT was also up-regulated in MAX-silenced cells at the mRNA level (Fig. 1*J*). Altogether, the results showed that low MAX levels result in MNT up-regulation at the mRNA and protein levels.

MNT binds and represses its own promoter in the presence of MAX

The above results showing that MNT down-regulation took place at the mRNA level prompted us to investigate whether MNT impairs the activity of its own promoter. Bioinformatic analysis of human, mouse, and rat *MNT* promoter regions revealed that there are two E-box sequences within 1 kb upstream from the transcriptional start site of *MNT* (one canonical E-box, CACGTG (E-box 1) and one noncanonical CATGTG (E-box 2)) that are conserved among these three different species (Fig. 2*A*). We then constructed a luciferase reporter carrying the 850-bp upstream region of the transcription start site from the human MNT gene. The construct was

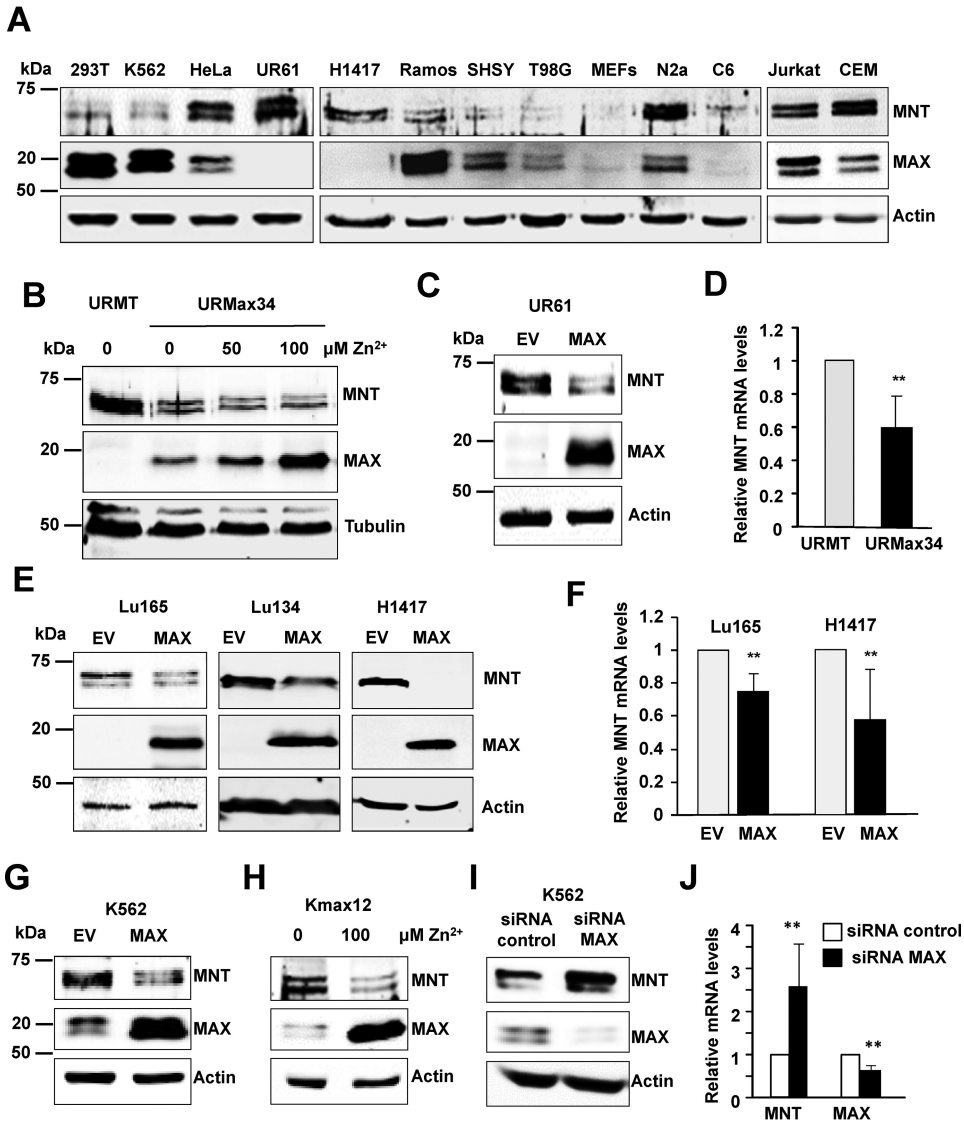

Figure 1. High MNT expression in MAX-deficient cells. *A*, cell lysates of the indicated cell lines were analyzed by immunoblot to determine the levels of MNT and MAX. β-Actin levels were determined as a protein-loading control. The MAX-deficient cell lines analyzed were UR61 (rat pheochromocytoma) and H1417 (human small cell lung carcinoma). The rest are MAX-expressing cells: HEK293T (human embryonic kidney, 293T); K562 (human chronic myeloid leukemia); HeLa (human cervical cancer); Ramos (human B-cell lymphoma); SH-SY5Y (SHSY, human neuroblastoma); T98G (human glioblastoma); mouse embryonic fibroblasts; Neuro-2a (N2a, mouse neuroblastoma); C6 (rat glioma); Jurkat (human T lymphoma); and CEM (human T leukemia). *B*, control URMT and URMax34 cells were treated for 24 h with 50 and 100 μM Zn^{2+}, and the MNT and MAX protein expression was determined by immunoblot. α-Tubulin levels were determined as a protein-loading control. *C*, levels of MNT and MAX determined by immunoblot in UR61 cells 24 h after transfection with a MAX expression vector or the empty vector pCEFL (*EV*). *D*, mRNA expression determined by RT-qPCR in URMT and URMax34 cells treated for 24 h with 100 μM Zn^{2+}. Data represent the mean ± S.D. from three independent experiments; **, $p < 0.05$. *E*, protein levels of MNT by immunoblot in Lu165, Lu134, and H1417 cells. The lysates were prepared 72 h after infection with MAX-expressing lentivirus or empty lentivirus (*EV*). *F*, MNT mRNA expression in Lu165 and H1417 determined 72 h after infection with MAX-expressing lentivirus or empty lentivirus (*EV*) determined by RT-qPCR. Data are shown as mean ± S.D. ($n = 3$); **, $p < 0.05$. *G*, MNT and MAX levels determined by immunoblot in K562 cells 24 h after transfection with a MAX expression vector. *H*, MNT and MAX levels determined by immunoblot in Kmax12 cells treated for 48 h with 100 μM Zn^{2+} to induce MAX expression. *I*, MNT and MAX protein expression analyzed by immunoblot in K562 48 h after transfection with siRNA against MAX gene. The results were reproduced in two experiments. *J*, MNT and MAX mRNA expression analyzed by RT-qPCR 48 h after transfection with siRNA against MAX gene. Data are shown as mean ± S.D. ($n = 4$); **, $p < 0.05$.

termed MNT–Luc (Fig. 2*B*). HEK293T cells (which express MAX) were transfected with the MNT–Luc and MNT expression vectors (or the corresponding empty vectors). The results showed that MNT overexpression led to a reduction in the luciferase activity (Fig. 2*C*, *left panel*), suggesting that MNT–MAX negatively regulates the *MNT* promoter. To determine the contribution of the two E-boxes in the MNT-mediated negative autoregulation, we constructed two reporters containing each of the E-boxes, termed E-box 2 MNT–Luc (containing the last 220 bp of the MNT–Luc reporter, which includes E-box 2) and E-box 1 MNT–Luc (containing the first 570 bp of the MNT–Luc reporter which includes E-box 1) (Fig. 2*B*). The luciferase assays in HEK293T cells suggested that the MNT promoter down-regulation depended on the E-box 2 (Fig. 2*C*, *left panel*).

We also investigated the activity of the *MNT* promoter in UR61 cells, which do not express MAX. UR61 cells were transfected with the MNT–Luc vector together with MNT and MAX expression vectors. The results also showed a decrease in the luciferase activity although less than in HEK293T cells (Fig.

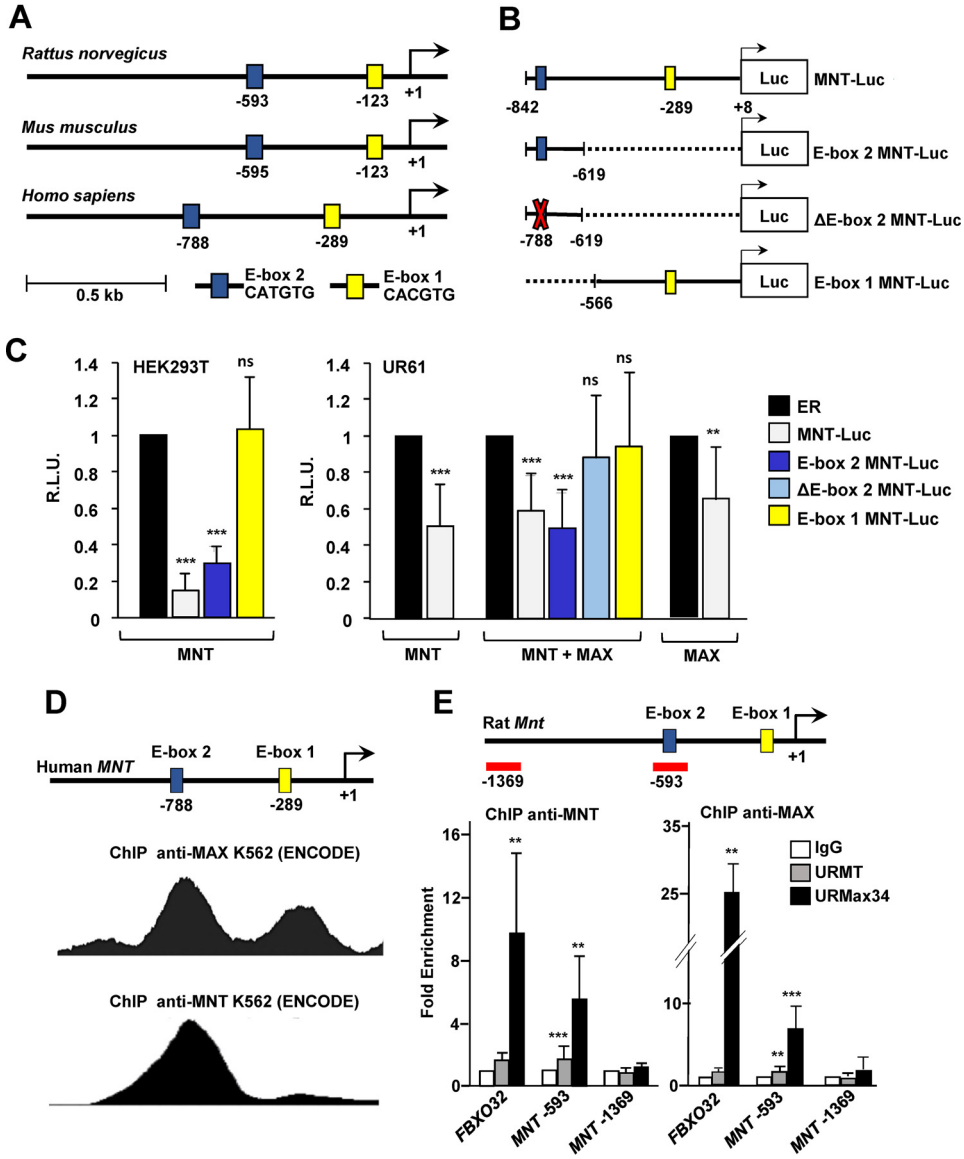

Figure 2. MNT represses its own promoter. *A*, schematic representation of human, rat, and mouse MNT promoters showing two conserved E-boxes. The coordinates correspond to the 5′-nucleotide of each E-box, using the UCSC genome browser. *B*, luciferase reporters driven by human MNT promoter generated in this work. *C*, luciferase assays in HEK293T and UR61, 24 or 36 h after transfection, respectively, with expression vectors for MNT and MAX. Results are expressed in relative luciferase units (*R.L.U.*) after normalizing each condition first to the luciferase empty reporter (*ER*; no promoter) and then to the empty expression vector of MNT and/or MAX. The data are shown as the mean ± S.D. of nine (for MNT-luc) or four independent transfections (for the rest of experimental points). ***, $p < 0.01$; **, $p < 0.05$; *ns*, nonsignificant. *D*, schematic representation of human MNT promoter showing the peaks for MAX and MNT on human K562 cell line as published by the ENCODE project. *E*, ChIP with anti-MNT (*left*) and anti-MAX (*right*) antibodies of URMT and URMax34 cells, both treated with 100 μM Zn^{2+} for 24 h. MNT and MAX binding to MNT gene promoter (below) was studied by qPCR at the amplicons shown with *red bars*. *MNT −593* corresponds to the region containing the E-box 2, and *MNT −1369* corresponds to an upstream region without E-boxes (negative control). An amplicon from Atrogin-1 (*FBXO32*) was used as positive control for MNT binding. The data are means ± S.D. ($n = 3$); ***, $p < 0.01$; **, $p < 0.05$.

2*C*, *right panel*). The expression of MNT alone also led to a decrease in the luciferase activity, suggesting that MNT can down-regulate the *MNT* promoter in UR61 cells in the absence of MAX. The repressive effect of MNT was stronger in HEK293T cells than in UR61 cells, which may be explained by the limited overexpression of MNT protein achieved in transfected UR61 cells (shown below). Co-transfection of *MNT* and *MAX* resulted in a decrease in the activity of both promoter constructs (MNT–Luc and E-box 2 MNT–Luc). We next constructed a reporter with a deletion of the −788 E-box (ΔE-box 2 MNT–Luc), and the results showed that in UR61 cells MNT had no effect on the activity of the mutant reporter (Fig. 2*C*, *right panel*), confirming that E-box 2, mapping at −788, was critical for MNT-mediated down-regulation of its own promoter.

Because MNT–MAX bind E-boxes in the promoters to repress transcription, we analyzed the ChIP-seq data published by the ENCODE project. The data revealed two regions bound by MAX in the human MNT promoter that encompass the two E-boxes (Fig. 2*D*). Interestingly, according to ENCODE, ChIP-seq for MNT also showed that MNT binds to the region encompassing E-box 2 in human K562 cells (Fig. 2*D*). We also analyzed the ChIP-seq peaks for MAX, MYC, and MXI1 proteins on the *MNT* promoter as published by the ENCODE project.

We looked at other human cell lines like H1ES, HeLa, NB4, A549, GM78, HEPG, SKSM, and IMR90. The analysis revealed that the three proteins presented peaks at the same positions near the transcription start site of the human MNT gene (Fig. S1*B*), suggesting that members of the MYC and MXD family bind and possibly regulate the promoter of *MNT*.

As MNT was significantly down-regulated when MAX was re-expressed, we hypothesized that MNT–MAX heterodimers might bind to the *MNT* promoter and down-regulate its own expression. To explore this hypothesis, a ChIP assay was performed with anti-MNT and anti-MAX antibodies in URMT and URMax34 cells treated with Zn^{2+}, which induces MAX in the URMax34 cells. We studied the −593 E-box of the rat *MNT* promoter, as well as a region of the *FBXO32* (*Atrogin-1*) promoter as a positive control for MNT binding (25). A region mapping at 1369 bp upstream on *MNT* transcription start site with no E-boxes was used as negative control. As shown in Fig. 2*E*, MNT and MAX bound to the *MNT* promoter in URMax34 cells. However, in the MAX-deficient control URMT cells, the binding of MNT to its promoter was very weak, but above that of the IgG controls. This weak binding could be responsible for the decreased promoter activity detected in the results shown of Fig. 2*C* in MNT-transfected UR61 cells. MNT and MAX were bound to the positive control *FBXO32*/*Atrogin-1* promoter in URMax34 but not in URMT control cells (Fig. 2*E*). These data show that MNT most likely binds to its own promoter as a heterodimer with MAX and suggest a possible negative regulation of *MNT*'s own expression.

Then, to explore the binding of MNT to other regions of the genome in the absence of MAX, we performed ChIP-seq experiments with an anti-MNT antibody in MAX-deficient URMT cells. We sequenced the immunoprecipitated chromatin and the inputs of three independent experiments. The results showed first that MNT bound very weakly to the promoter of *MNT* in the absence of MAX, while stronger binding was detected in other genes like *CCNG2* (Table S1). This indicates that MNT binds to DNA even in the absence of MAX. The peaks of MNT bound to the regulatory regions of some of these genes (*MNT*, *FBXO32*/*Atrogin-1*, *CCNG2*, *CDK12,* and *ERCC6*) are shown on Fig. S2*A*. To evaluate the possible transcriptional effect of MNT binding to these genes, we knocked down *MNT* in URMT and URMax34 cells through short-hairpin constructs and checked their expression by RT-qPCR. The results showed that upon MNT knockdown, the mRNA expression of these genes increased (Fig. S2*B*), indicating that MNT binds to their promoters to repress their expression even in the absence of MAX.

Ontology analysis of the genes obtained in our ChIP-seq experiments reveals that MNT-bound genes are involved in cell cycle, DNA replication, and regulation of gene expression (Fig. S3*A*). We then analyzed whether there were any DNA motifs that were over-represented in the regions bound by MNT. The results revealed that MNT binds to regions with E-boxes in the absence of MAX but also to regions containing DNA-binding motifs for other transcription factors such as forkhead factors, SMAD, VDR, and TBXT (Fig. S3*B*).

MNT knockdown impairs cell proliferation in MAX-deficient cells

We next asked for a possible biological effect of MNT on cell proliferation in the UR61 MAX-deficient cells. We decided to knock down *MNT* through siRNAs. For this, we used expression vectors for two short-hairpin constructs against the rat MNT gene. These shMNT constructs efficiently reduced MNT levels and were termed shMNT-1 and shMNT-2 (Fig. 3*A*). The vectors also carried a puromycin-resistance gene. UR61 cells were transiently co-transfected with the shMNT constructs (or the empty vector) and a GFP expression vector in a proportion of 5:1 (shMNT/GFP vector) to ensure that the GFP-positive cells also incorporated the shMNT plasmid. Six days after transfection, the fraction of GFP-positive cells was analyzed by flow cytometry. The results showed that the fraction of GFP-positive cells was clearly reduced in cells with depleted MNT (Fig. 3*B*), suggesting that MNT loss resulted in impaired cell proliferation. In a second approach, we transfected the UR61 cells with the shMNT constructs and counted viable cells after 3, 7, and 12 days of transfection. As shown in Fig. 3*C*, MNT-silenced UR61 cells grew slower than controls. We also performed clonogenic assays in UR61 transfected with the shMNT and/or a MAX expression vector (in 1:3 proportions to ensure that the shMNT-containing cells had also incorporated the MAX vector) as well as the empty vectors. Then, 24 h after transfection puromycin was added and after selection, the colonies were stained with crystal violet, and the dye was solubilized and quantified. The data showed that MNT depletion provoked a dramatic growth inhibition (Fig. 3*D*). We conclude that MNT depletion impairs cellular proliferation in MAX-deficient cells. This was a striking result as it demonstrates a MAX-independent biological function of MNT. We also observed that UR61 cells overexpressing the MAX protein grew slower than the control (Fig. 3*D*), confirming the effect previously reported for the MAX-deficient PC12 pheochromocytoma cells (UR61 parental cells) (20). In addition, when MNT silencing was accompanied by MAX-enforced expression, the inhibition of UR61 cell proliferation was stronger (Fig. 3*D*). Consistent with the anti-proliferative effects of MNT depletion, we failed to generate stable MNT-silenced UR61 cell lines. To generate UR61 cells with MNT overexpression, we transfected UR61 with MNT expression vectors, but we were not able to detect a significant increase in MNT protein levels upon transfection. However, MNT protein was readily detected by immunoblot when the transfected cells were treated with the proteasome inhibitor bortezomib (Fig. S4*A*).

This could be explained if in the MAX-deficient cells the MNT levels are already high and enforced expressed MNT is degraded by the proteasome. In fact, some increase in the levels of MNT was detected when MNT was transfected in MAX-expressing URMax34 cells (Fig. S4*B*) or when MNT was co-transfected with MAX in UR61 cells (Fig. S4*C*).

Because the depletion of MNT impairs cell proliferation of UR61 cells, we wondered whether apoptosis is involved in this process. We found that the fraction of cells with a sub-G_0 amount of DNA was higher in cells transfected with the shMNT vector (Fig. 3*E*) and an increase in annexin V–positive

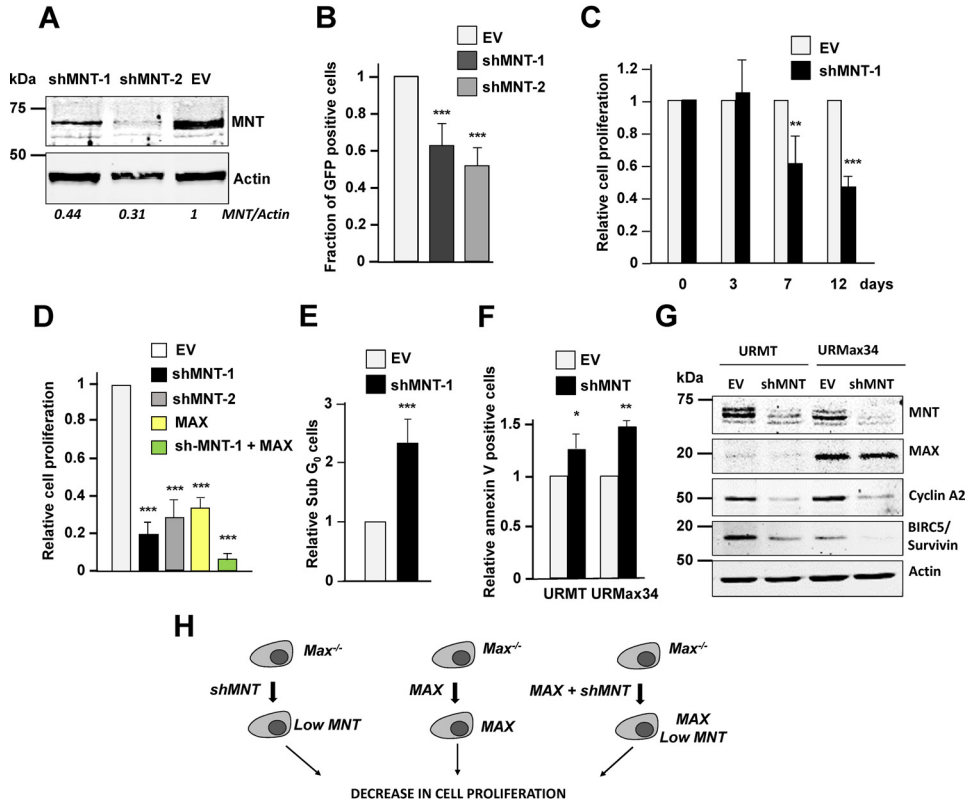

Figure 3. MNT knockdown impairs cell proliferation in MAX-deficient cells. *A*, silencing of MNT by short-hairpin constructs. URMT cells were transfected with vectors encoding shMNT-1 and shMNT-2. 24 h after transfection, the cells were treated with puromycin (0.3 μg/ml), and 72 h after transfection the cells were lysed, and the levels of MNT were analyzed by immunoblot. β-Actin levels were determined as protein-loading control. *B*, fraction of GFP-expressing UR61 cells assessed by flow cytometry 7 days after co-transfection with GFP and shMNT vectors (in proportion 1:5) and analyzed by flow cytometry. The data are shown as mean $\pm$ S.D. ($n = 3$); ***, $p < 0.01$. *C*, cell proliferation determined by cell counting at 3, 7, and 12 days after transfection of shMNT-1 or the empty vector pLKO. The data are shown as relative mean values $\pm$ S.D. ($n = 3$); ***, $p < 0.01$; **, $p < 0.05$. *D*, cell growth determined by crystal violet staining in UR61 cells transfected with the indicated vectors. After 15 days of puromycin selection, the colonies were stained with crystal violet, and the dye was solubilized and quantified by absorbance at 595 nm. *EV*, empty vector (pLKO for shMNTs and pCEFL for MAX). ***, $p < 0.01$. Data show mean values $\pm$ S.D. from three (*EV* and *MAX*) or six independent experiments (*shMNTs*). *E*, fraction of sub-G_0 UR61 cells transfected with the shMNT-1 vector relative to the empty vector. Cells were fixed and stained with propidium iodide at day 6 post-transfection and puromycin selection. The percentage of cells containing less than 2C DNA content was determined by flow cytometry. The data are mean values $\pm$ S.D. ($n = 3$); ***, $p < 0.01$. *F*, quantification of annexin V-bound URMT and URMAX cells 4 days after transfection with a mixture of shMNT-1 and shMNT-2 (or the empty vector), and 24 h of treatment with 100 μM Zn^{2+}. The data are mean values $\pm$ S.D. ($n = 3$); **, $p < 0.05$; *, $p < 0.1$. *G*, levels of MNT determined by immunoblot in URMT and URMax34 cells 72 h after transfection with a mixture of shMNT-1 and shMNT-2 or the empty vector and treated for 12 h with 100 μM Zn^{2+}. MAX, cyclin A2, and survivin (BIRC5) were also determined. *H*, summary of the effects of MNT knockdown and MAX overexpression in the UR61 model.

cells (Fig. 3*F*). The levels of cyclin A (a marker of cell proliferation) and survivin/BIRC5 (a marker of both proliferation and apoptosis) in URMT and URMax34 were analyzed by immunoblot. The results showed a decrease in survivin and in cyclin A in cells with depleted MNT, both in MAX-deficient cells (URMT) and in MAX-expressing cells (URMax34) (Fig. 3*G*). However, we did not detect cleavage of PARP1, a marker of apoptosis (data not shown). These results suggest that the depletion of MNT leads to cell proliferation arrest even in the absence of MAX, which can be partially due to the induction of apoptosis. In addition, restoration of MAX expression also impairs proliferation The results are summarized in Fig. 3*H*.

MNT regulates gene expression in MAX-deficient cells

Because the data shown above indicated that MNT knockdown in UR61 cells leads to growth arrest, we set out to study whether MNT regulates the transcriptional program in the absence of MAX. For this purpose, we determined the transcriptomes upon MNT depletion in cells with and without MAX. URMT and URMax34 cells were transfected with the short-hairpin RNA construct against the rat MNT gene (shMNT-1) or the empty vector as control in two different biological replicates. We first checked the depletion of MNT mRNA in the two replicates used for RNA-seq upon transfection of the shMNT-1 construct in URMT and URMax34 cells. URMT and URMax34 cells were transfected with the shMNT-1 construct, and 2 days after transfection, cells were treated with Zn^{2+} for 24 h. The results indicated the induction of MAX mRNA expression in URMax34 as well as significant MNT mRNA depletion in the two independent transfections (Fig. 4*A*). These RNA preparations were submitted for next generation sequencing, RNA-seq . The data were then processed bioinformatically as described under "Experimental procedures" to obtain the expression values of each experimental replicate. For all of the different comparisons, we grouped the genes that were up-regulated and down-regulated in both biological replicates considering a log2 RPKM fold change higher than 0.7 or smaller than -0.7 (1.6$\times$ or 0.6$\times$ fold change, respectively) of the corresponding control and a p value <0.1. The heat maps of the gene expression signatures clearly showed

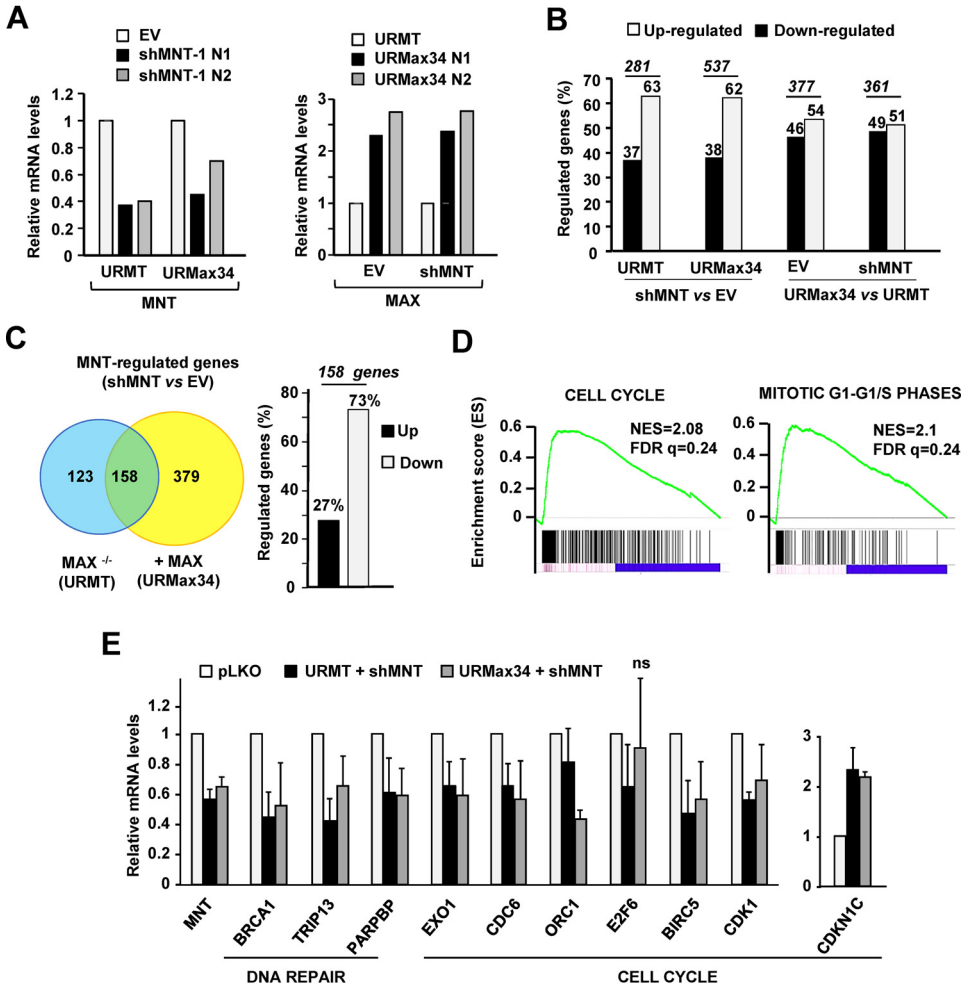

Figure 4. Gene expression changes in MNT knockdown cells. *A*, mRNA expression of MNT and MAX in URMT and URMax34 cells lysed 72 h after transfection with shMNT-1 and 24 h of treatment with 100 μM Zn^{2+}. The experiments were performed in duplicated (*N1* and *N2*) biological replicates. These RNAs were subjected to RNA-seq. *B*, percentage of up-regulated and down-regulated genes in cells transfected with the shMNT or pLKO (empty) vectors in URMT and URMax34 cells, as indicated at the *bottom*. The number of genes regulated comparing the different samples are indicated at the *top* of the figure. The gene inclusion criteria used was a change in mRNA level $\geq$0.7 or ≤ -0.7 log2 fragments per kilobase million fold change. The RNA-seq data are from two independent experiments. The genes regulated in the different comparisons are listed in Tables S2 and S3. *C*, Venn diagram showing the genes that are regulated by MNT in MAX-deficient (*URMT*) or MAX-expressing cells (URMax34). The *graph at the right* shows the number of up- or down-regulated genes in the group of overlapping genes. *D*, Gene Set Enrichment Analysis (GSEA) plots showing "cell cycle" and "mitotic G_1–G_1/S phases" KEGG pathways enriched in the genes regulated upon MNT depletion in URMT cells. Normalized Enriched Score and False Discovery Rates are shown for each gene set. *E*, mRNA expression regulation due to MNT silencing in genes selected after the RNA-seq data analysis. URMT and URMax34 were transfected with shMNT-2 or empty vector (*pLKO*). After 48 h cells were treated for 24 h with 100 μM Zn^{2+}, and total RNA was prepared, and mRNA levels of the indicated genes were determined by RT-qPCR. The selected genes are involved in DNA repair or cell cycle as indicated. The data are represented are means $\pm$ S.D. ($n = 3$ independent transfection experiments). In all cases except E2F6 in URMax34 with shMNT: $p < 0.05$. *ns*, non-significant.

that the depletion of MNT in both URMT and URMax34 induced gene expression changes (Fig. S5) indicating that MNT can be involved in transcriptional regulation without the concourse of MAX. Specifically, 281 genes were regulated upon MNT depletion in MAX-deficient URMT cells (Table S2) and 537 genes in MAX-expressing cells (*i.e.* URMax34 treated with Zn^{2+}) (Table S3). Of those, ~62% of the genes were down-regulated upon MNT depletion in both cell lines (Fig. 4*B*). In the presence of MAX (URMax34 cells), MNT regulates more genes than in the absence of MAX (URMT cells): 537 *versus* 281 genes (Fig. 4*B*). In addition, the URMax34 *versus* URMT gene expression signature heat maps also showed that the expression of MAX induced gene transcriptional changes independently of MNT depletion (Fig. S5). Specifically, 377 genes were found to be differentially expressed when comparing URMax34 and URMT cells (Table S4) and 361 genes when comparing URMax34 and URMT cells depleted of MNT (Table S5). Among MAX-regulated genes, roughly half of the genes were down-regulated (Fig. 4*B*). Importantly, the comparison between the lists of differentially expressed genes upon MNT depletion in cells without MAX (URMT) and with MAX (URMax34) revealed 158 shared genes (27% up-regulated and 73% down-regulated) in the two biological replicates (Fig. 4*C*). These common genes are listed in Table S6. Thus, 56% (158/281) of the genes regulated by MNT in URMT (without MAX) cells are also regulated in URMax34 cells (when MAX is expressed). However, the 30% (158/537) of the genes regulated in URMax34 cells (with MAX) are also regulated in the MAX-less URMT cells (Fig. 4*C*). Furthermore, we generated a dot plot graph with the RPKM values of the differentially expressed transcripts obtained in our RNA-seq data in URMT and URMax34 cells upon MNT knockdown (Fig. S6). The graph

showed that the transcriptional changes induced by *MNT* depletion followed the same pattern in the URMT and URMax34 cells suggesting that the presence of MAX did not affect dramatically the direction of MNT-transcriptional regulation in the UR61 cells. The lists of differentially-regulated genes upon MNT knockdown were compared with the gene sets derived from the biological process gene ontology (based on MsigDB platform, http://software.broadinstitute.org/gsea/msigdb),[11] and the comparison showed the enrichment in cell cycle-related pathways in both cell lines (Fig. S7*A*). In addition, the analysis with the Gene Set Enrichment Analysis (GSEA) platform showed that the gene expression signature in URMT cells upon MNT depletion was associated with the cell cycle as the two most enriched pathways (Fig. 4*D*). A list of these genes is shown in Fig. S7*B*. Altogether, the functional analysis of the gene transcriptional signatures is consistent with the inhibition of cell proliferation elicited by MNT silencing (Fig. 3).

Thus, to explain and confirm the effects of MNT knockdown on UR61 cell proliferation, we selected several genes involved in cell cycle and DNA replication and repair processes in which expression was changed according to the RNA-seq data to analyze their expression by RT-qPCR. URMT and URMax34 cells were transfected with the shMNT-2 construct and the empty vector following the same conditions as used for the RNA-seq experiment. Fig. 4*E* shows that genes involved in the cell cycle, DNA replication, and DNA repair were down-regulated upon silencing of *MNT* except *CDKN1C* (p57, a cell cycle inhibitor), which was up-regulated. Altogether, the results are consistent with the negative effect of MNT depletion on cell proliferation in UR61 cells.

MNT localizes in the cytoplasm of MAX-deficient cells

In an attempt to explain the higher MNT levels observed in UR61 cells as compared with the MAX-expressing counterpart, we next examined the subcellular localization of the excess MNT present in MAX-deficient cells. URMT and URMax34 cells were treated with Zn^{2+} to induce MAX, and we performed a cytoplasmic and nuclear fractionation to analyze MNT levels. In control URMT cells, MNT protein was found in the nuclear fraction, as expected, but also at similar levels in the cytoplasm. In contrast, in URMax34-expressing MAX, MNT protein was found only in the nucleus (Fig. 5*A*), which is the localization typically described for MNT (26). We were not able to use untreated URMax34 cells as a control as they express some MAX even in the absence of Zn^{2+} (Fig. 1*B*). Cytoplasmic MNT was also observed in H1417 cells, human cells deficient in MAX (Fig. 5*A*). As a control, the localization of MNT was also analyzed in HEK293T cells, which express the MAX protein. Cytoplasmic/nuclear fractionation revealed that MNT and MAX were localized in the nucleus but not in the cytoplasm of HEK293T cells (Fig. 5*A*). As controls for nuclear and cytoplasmic proteins, we used SIN3B and RhoGDI, respectively (Fig. 5*A*). To test whether the localization of MNT depended on MAX, we silenced the MAX protein in K562 cells with siRNA, and we carried out cytoplasmic/nuclear fractionation. In control K562 cells, MNT and MAX were mainly localized in the nucleus. In contrast, in MAX-depleted cells, a significant amount of MNT was found in the cytoplasm of K562 cells. As controls for nuclear proteins, we used MYC and CTCF (Fig. 5*B*). It is noteworthy that nuclear MNT levels were similar in URMT and URMax34, as well as in control K562 and MAX-depleted K562 cells. Taken together, the data indicate that the absence of MAX leads to an up-regulation of MNT protein and that the excess of MNT appears to be accumulated in the cytoplasm.

MNT interacts with MLX in the absence of MAX

Besides MAX, MNT can also bind the HLH protein MLX (6, 27). Therefore, MNT would have two partners in UR61-expressing MAX but only one in the absence of MAX, and alternatively, MNT could form homodimers, as schematized in Fig. 5*C* and previously described *in vitro* (5). To investigate whether the MNT–MLX interaction also takes place in UR61, we transfected MLX–Flag into URMT cells, and 48 h later lysates were immunoprecipitated with anti-MLX and anti-MNT antibodies. The immunoprecipitates were analyzed by immunoblot, and the data demonstrated that MNT interacted with MLX in UR61 cells (Fig. 5*D*). We next studied this interaction in URMax34 cells treated with Zn^{2+}, *i.e.* cells expressing MAX. The immunoblot results showed that MNT and MLX also interacted between them, but the interaction was weaker when MAX expression was induced by Zn^{2+}. Thus, the data suggest that, at least in our experimental conditions, MNT–MAX dimers were formed preferentially than MNT–MLX dimers (Fig. 5*E*). To confirm the MNT–MLX interaction in URMT cells, we prepared a HA-tagged MNT mutant with a deletion of the HLH domain of mouse MNT, termed ΔbHLH MNT-HA (Fig. 5*F*). This mutant and the WT counterpart were transfected into URMT and the corresponding lysates were immunoprecipitated with anti-HA. The results showed that HLH domain is required for the MNT–MLX interaction (Fig. 5*G*). As a proof of concept, we performed the same co-immunoprecipitation in HEK293T, obtaining the same result (Fig. 5*H*).

In contrast to MAX, MLX is found both in the nucleus and cytoplasm (28). By immunoblot analysis, it was found that MLX was present in the cytoplasm and, at a lesser extent, in the nucleus of URMT cells (Fig. 5*I*). Next, we prepared nuclear and cytoplasmic fractions of URMT cells and studied by immunoprecipitation with anti-MNT and anti-MLX antibodies whether MNT and MLX interacted in these cell compartments. The results showed that MNT and MLX co-immunoprecipitated in both nuclear and cytoplasmic fractions (Fig. 5*J*).

As mentioned above, it is described that MNT can form homodimers *in vitro* and in two-hybrid experiments in yeasts (4, 5). Thus, another possibility is that MNT acts as a transcription factor by forming homodimers. This homodimerization has not been demonstrated in animal cells, so we tested this in HEK293T and UR61 cells. We first co-transfected HEK293T cells with GFP–MNT and Flag–MNT constructs and immunoprecipitated with anti-GFP antibody. The immunoblot analysis demonstrated the presence of the smaller Flag–MNT protein in the material immunoprecipitated with anti-GFP indicating that MNT forms homodimers in the cell (Fig. 6*A*). As expected, both

[11] Please note that the JBC is not responsible for the long-term archiving and maintenance of this site or any other third party hosted site.

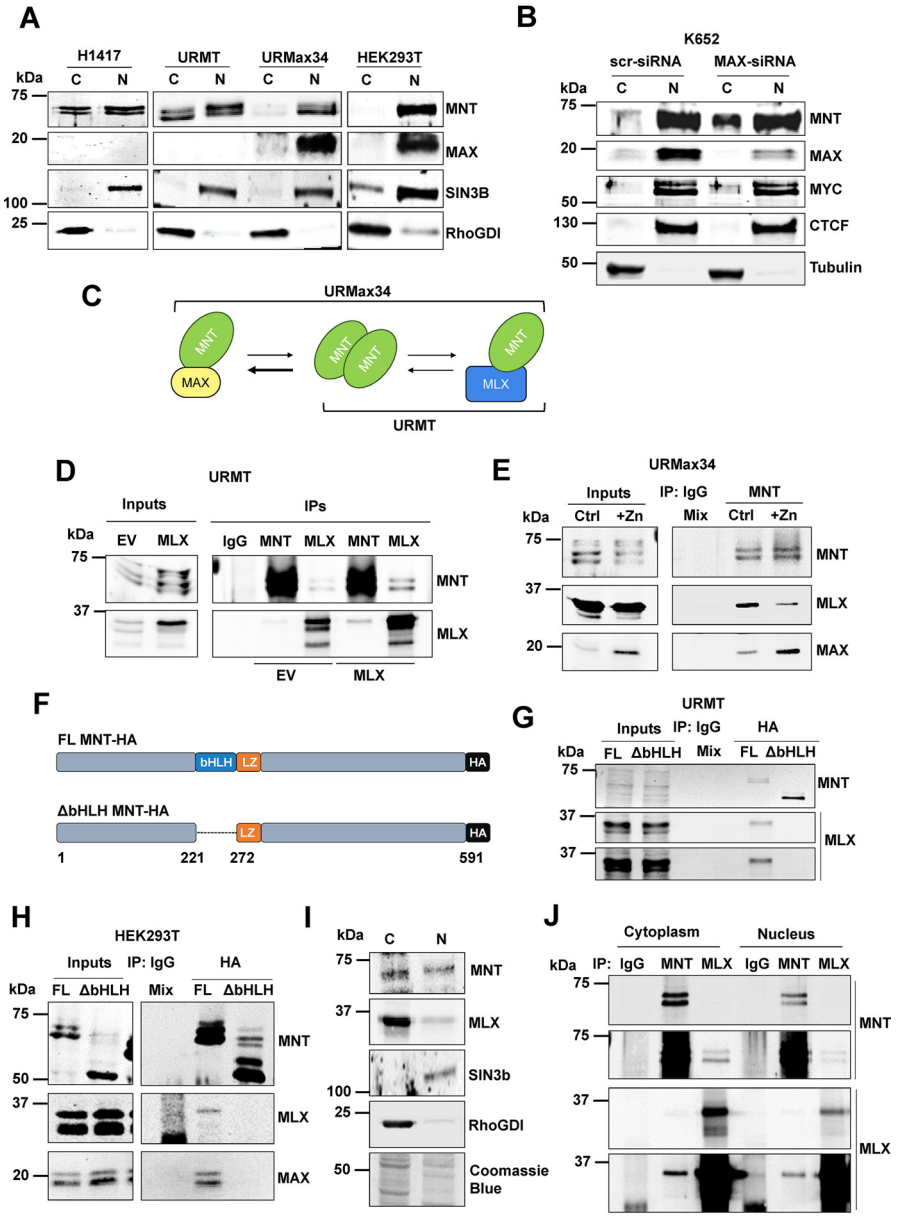

Figure 5. MNT subcellular localization and interaction with MLX depends on MAX. *A*, cell extracts were subjected to cytoplasmic/nuclear fractionation in H1417 (human lung cells deficient in MAX), HEK293T, URMT, and URMax34 treated for 24 h with 100 μM Zn^{2+} to induce MAX. The levels of MNT and MAX were determined in each fraction by immunoblot. SIN3B and RhoGDI (ARHGDIA) were used as nuclear and cytoplasmic markers, respectively. *C* refers to cytoplasmic fraction, and *N* refers to nuclear fraction. *B*, K562 cells were transfected with siRNA against the *MAX* gene, and 48 h later cell extracts were prepared and subjected to cytoplasmic/nuclear fractionation. The expressions of MAX, MNT, and MYC were analyzed by immunoblot. The expressions of CTCF and α-tubulin were analyzed as a control for nuclear and cytoplasmic proteins, respectively. *scr-siRNA*, control scrambled siRNA. *C*, working hypothesis of the interactions of MNT to test in URMT (MAX-less) and URMax34 (expressing MAX when treated with Zn^{2+}). *D*, URMT cells were transfected with an MLX expression vector or the empty vector (*EV*). 48 h after transfection, total cell lysates were prepared and precipitated with anti-MNT or anti-MLX antibodies, as well as unspecific IgG. The presence of MNT and MLX in the immunoprecipitates was detected by immunoblot. *E*, effect of MAX on the MNT–MLX interaction. URMax34 cells were transfected with an MLX expression vector, and 48 h after transfection, cells were treated with 100 μM Zn^{2+} for 24 h to induce MAX or left untreated (*Ctrl*). Total cell lysates were immunoprecipitated (*IP*) with anti-MNT. As a control, a mixture of lysates from cells treated and untreated with Zn^{2+} (*Mix*) was immunoprecipitated with unspecific IgG. The presence of MNT, MLX, and MAX in the immunoprecipitates was analyzed by immunoblot. *F*, schematic representation of the FL and the deletion mutant ΔbHLH MNT-HA used in subsequent experiments. The Sin3-interacting domain, bHLH, LZ domains, HA tag, and amino acids of the murine protein are indicated. *G*, URMT cells were co-transfected with a vector expressing MLX and the constructs shown in *F*, as indicated at the *top*. 48 h after transfection, cell lysates were prepared, and the cells were immunoprecipitated with mouse anti-HA antibody to pull down the exogenous MNT proteins constructs. The presence of MNT and MLX in the immunoprecipitates was analyzed by immunoblot. As a control, a mixture of lysates from cell transfected with FL MNT and ΔbHLH MNT (*Mix*) were immunoprecipitated with unspecific IgGs. *H*, HEK293T cells were co-transfected with a vector expressing MLX and the constructs shown in *F*, as indicated at the *top*. 24 h after transfection, cell lysates were prepared, and the cells were immunoprecipitated with mouse anti-HA antibody to pull down the exogenous MNT. As a control, a mixture of lysates from cells transfected with FL MNT and ΔbHLH MNT (*Mix*) were also immunoprecipitated with unspecific IgGs. The presence of MNT and MLX in the immunoprecipitates was detected by immunoblot. MAX co-IP was determined as a positive control. *I*, MLX localization in UR61 cells. Nuclear (*N*) and cytoplasmic (*C*) extracts were prepared from URMT cells as described under "Experimental procedures," and the levels of MNT and MLX were determined in each fraction by immunoblot. SIN3B and RhoGDI (ARHGDIA) were used as nuclear and cytoplasmic markers, respectively. A picture of the gel stained with Coomassie Blue after transference is also shown as an indicator of the total amount of proteins in the cytoplasmic and nuclear fractions. *J*, interaction between MNT and MLX in the nucleus and cytoplasm. URMT cells were transfected with a MLX expression vector, and 48 h later nuclear and cytoplasmic extracts were prepared and immunoprecipitated with anti-MNT or anti-MLX antibodies. The levels of MNT and MLX in the immunoprecipitates were assayed by immunoblot.

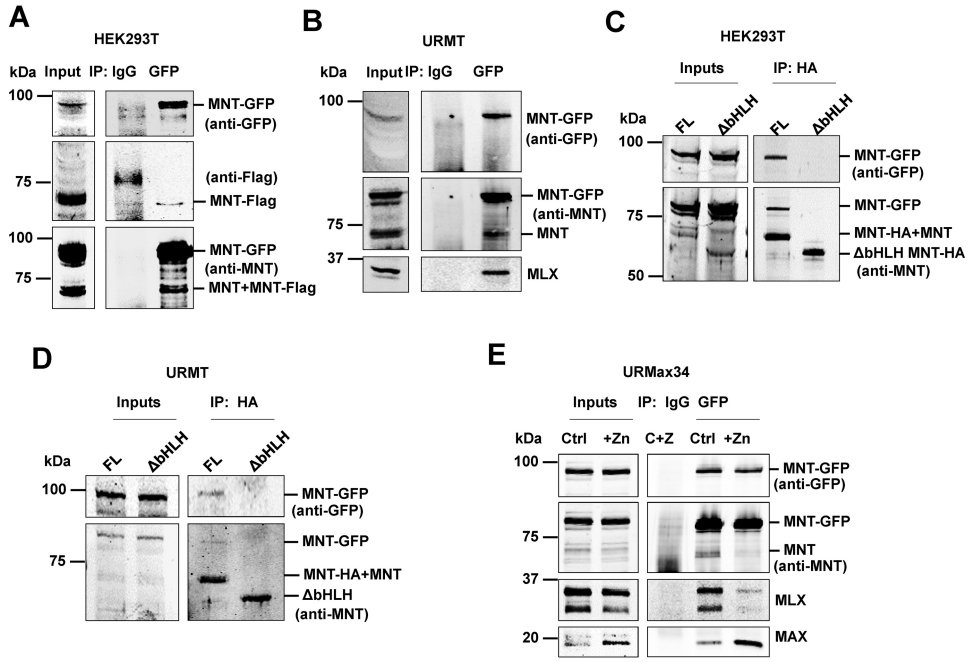

Figure 6. MNT homodimerization in UR61 cells. *A,* HEK293T cells were co-transfected with a GFP–MNT and MNT–Flag expression vectors, and 24 h later lysates were prepared and immunoprecipitated (*IP*) with an anti-GFP antibody. MNT–GFP and MNT–Flag were detected with the antibodies indicated at the *right side*. As a control, lysates were precipitated with unspecific IgG. The antibodies used in each immunoblot are indicated at the *right*. The results were reproduced in two immunoprecipitations. *B,* URMT cells were infected with lentivirus encoding a MNT–GFP, and 72 h later were transfected with MNT–Flag and treated with 15 nM bortezomib for 12 h before harvesting. 48 h after transfection, lysates were prepared and immunoprecipitated with anti-GFP antibody. The presence of MNT–GFP, MNT, and MLX in the immunoprecipitates was assessed by immunoblot. The antibodies used in each immunoblot are indicated at the *right*. The results were reproduced in two experiments. *C,* HEK293T cells were co-transfected with expression vectors for MNT–GFP and expression vectors for FL MNT or ΔbHLH MNT (shown in Fig. 5*F*) as indicated at the top of each lane. 24 h later, lysates were prepared and immunoprecipitated with anti-HA antibody. The levels of MNT–GFP and MNT were determined by immunoblot using anti-GFP and polyclonal anti-MNT antibody. *D,* URMT cells were infected with lentivirus encoding a GFP–MNT and 72 h later transfected with expression vectors for full-length (*FL*) MNT or ΔbHLH MNT as indicated at the *top of each lane*. 48 h after transfection, cell lysates were prepared and immunoprecipitated with anti-HA to pull down the transfected MNT proteins. The levels of MNT–GFP and MNT were determined by immunoblot using anti-GFP and polyclonal anti-MNT antibody. *E,* URMax34 cells were transfected with a MNT–GFP expression vector, and 48 h after transfection cells were left untreated or treated with 100 μM Zn^{2+} for 24 h to induce MAX. Then total cell lysates were prepared and immunoprecipitated with anti-GFP. As a control, a mixture of lysates from cells treated and untreated with Zn^{2+} was immunoprecipitated with unspecific IgG. The presence of MNT, MLX, and MAX in the immunoprecipitates was analyzed by immunoblot.

big and small MNT forms were detected when the immunoblots were analyzed with anti-MNT antibody. The results suggested the presence of homodimers between GFP–MNT and Flag–MNT in HEK293T cells. As a control, the lysates were immunoprecipitated with anti-MAX antibody, and both MNT and GFP–MNT were found to be bound to MAX (data not shown).

Next, we investigated the MNT homodimerization in the UR61 system. URMT cells were infected with lentiviral particles containing the GFP–MNT construct, immunoprecipitated with the anti-GFP antibody, and the immunoprecipitates analyzed by immunoblot with anti-MNT antibody and anti-GFP antibodies. The results showed that endogenous MNT was present in the immunoprecipitates with anti-GFP (Fig. 6*B*), suggesting that MNT forms homodimers in human HEK293T cells and in MAX-deficient rat URMT cells. As MNT dimerization in yeast two-hybrid assays depends on the bHLH-LZ (4, 5), we wondered whether HLH was involved in the homodimerization of MNT in our system. We transfected HEK293T cells with HA-tagged MNT constructs that lack the bHLH region (ΔbHLH MNT) (Fig. 5*F*) or the WT version together with GFP–MNT constructs, and we carried out immunoprecipitations with anti-HA antibodies that should only recognize the HA-tagged proteins. The immunoblot analysis of the immunoprecipitates revealed that ΔbHLH MNT was unable to interact with GFP–MNT (Fig. 6*C*). The same experiment was performed in URMT cells, and the same result was observed, *i.e.* GFP–MNT bound to WT MNT–HA but not to the ΔbHLH form (Fig. 6*D*). We conclude that MNT homodimerizes through the bHLH domain, as expected. We also wondered whether MNT preferentially binds to MAX or to MLX than to MNT itself. For this, we immunoprecipitated with the antibodies anti-GFP and lysates of URMax34 cells transfected with GFP–MNT that were untreated or treated with Zn^{2+} (to induce MAX). The levels of MAX and MLX after the immunoprecipitation assay were determined by immunoblot, and the results showed that when MAX and MLX are expressed, MNT preferentially binds to MAX than to MLX or MNT (Fig. 6*E*). Altogether, the results indicate that in URMT cells, MNT can form homodimers or heterodimers with MLX, whereas in URMax34 (in the presence of Zn^{2+}), MNT mainly forms heterodimers with MAX.

The former results showing that MNT can form homodimers open the possibility that in MAX-less cells, MNT can regulate gene expression either as a homodimer or as a heterodimer with MLX. To investigate this, we knocked down both MNT and MLX each with two short-hairpin constructs, in URMT cells (MAX-less) and URMax34 cells (with MAX) and

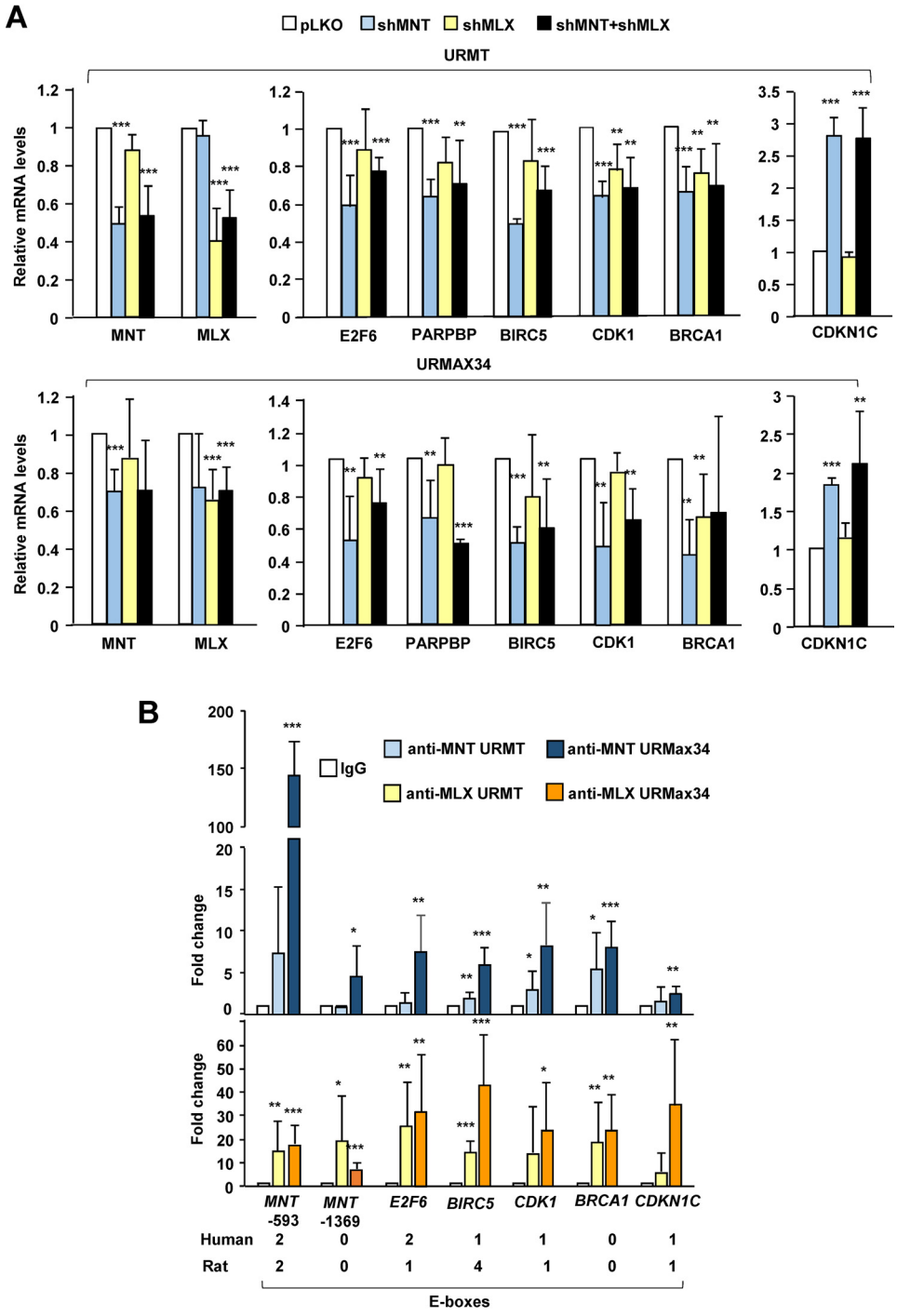

Figure 7. Gene expression changes in MNT and MLX knockdown cells. *A,* mRNA expression regulation due to MNT and MLX silencing in genes selected after the RNA-seq data analysis. URMT (*upper panel*) and URMax34 cells (*lower panel*) were transfected with a mixture of shMNT-1 and shMNT-2 and/or shMLX constructs as indicated. 48 h after transfection, cells were treated for a further 24 h with 100 μM Zn^{2+}, and total RNA was prepared, and mRNA levels of the indicated genes were determined by RT-qPCR. The data are shown as mean ± S.D. ($n = 3$). ***, $p < 0.01$; **, $p < 0.05$. *B,* ChIP with anti-MNT (*upper panel*) and anti-MLX (*lower panel*) antibodies of URMT and URMax34 cells, both treated with 100 μM Zn^{2+} for 24 h. The genes were those validated from the RNA-seq in *A* and showing a peak of MNT binding in the ENCODE dataset for the K562 cell line. The binding of MNT and MLX was analyzed by qPCR in the amplicons shown in Fig. S9*B*. The data are means ± S.D. ($n = 3$); ***, $p < 0.01$; **, $p < 0.05$; *, $p < 0.1$. PARPBP was not included as it does not show any MNT peaks in ENCODE. The presence of E-boxes in the regions bound by MNT in human K562 (according to ENCODE dataset) and in the corresponding regions in rat genome is indicated at the *bottom*.

determined the expression of some genes that, according to Fig. 4*E*, showed differential expression upon silencing of *MNT*. The depletion of MNT and MLX was confirmed at the mRNA (Fig. 7*A*) and protein levels (Fig. S8*A*). MLX knockdown led to retarded proliferation (Fig. S8*B*) to a similar extent as in MNT depletion. The RT-qPCR analysis showed that in MAX-deficient cells, upon MNT knockdown, *CDKN1C/p57* was up-regulated, whereas *E2F6*, *PARPBP*, and *BIRC5* were down-regulated, as already shown in Fig. 4. However, the expression changes of these four genes were not significantly modified

when MLX was depleted or when both MNT and MLX were concomitantly depleted, suggesting that MNT could regulate these genes as homodimers (Fig. 7*A*). In contrast, *CDK1* and *BRCA1* were down-regulated when *MNT* was silenced but also when *MLX* was silenced (Fig. 7*A*). However, the expression of *CDK1* and *BRCA1* was not down-regulated further when both *MNT* and *MLX* were silenced. This suggests that both MNT–MNT and MNT–MLX dimers could be regulating the transcription of these genes.

To check whether the transcriptional changes observed upon *MNT* and *MLX* silencing were caused by a direct regulation driven by MNT and/or MLX, we performed ChIP–PCR assays in URMT and URMax34 cells after 24 h of stimulation with Zn^{2+} (*i.e.* cells in the absence or presence of MAX). From the genes analyzed by RT-qPCR (Fig. 7*A*), we chose to analyze the genes that showed a peak for MNT binding in the K562 ChIP-seq published in the ENCODE project: *E2F6, BIRC5, CDK1, BRCA1,* and *CDKN1C*. Then, primers for amplifying these regions in the rat genome were designed, and the presence of E-boxes in the amplicons was confirmed in all but *BRCA1* (Fig. 7*B*, *bottom*). The coordinates of the E-boxes in human and rat genomes are shown in Fig. S9*A*. The ChIP–PCR results showed that in the absence of MAX (in URMT cells), MLX and MNT were bound to the promoter of *BRCA1* and *BIRC5* (Fig. 7*B*).

Together with the results of Fig. 7*A*, the data suggest that these genes are regulated by MNT homodimers and possibly MNT–MLX dimers in the case of *BRCA1*, as the expression of this gene is affected by MLX knockdown. In the presence of MAX (URMax34 treated with Zn^{2+}), both MNT and MLX were bound to the promoters of the selected genes. MNT showed a much stronger signal in URMax34 cells that in the absence of MAX (Fig. 7*B*), suggesting a higher affinity of MNT–MAX to DNA and/or higher stability of the heterodimers *versus* MNT homodimers, as already shown in Fig. 4. We also performed a ChIP–PCR with anti-MAX in the same genes and amplicons in URMax34 cells and (as a negative control) in URMT. The results showed that MAX was bound to all promoters, but the signal in *BIRC5* and *BRCA1* was not statistically significant (Fig. S9*B*). Altogether, the data identified genes involved in cell cycle regulation and survival that are directly regulated by MNT–MNT or MNT–MLX dimers.

Discussion

In this study, we report several novel findings. (i) MNT is required for optimum proliferation even in the absence of MAX. (ii) In the absence of MAX, MNT expression is elevated, and a significant fraction localizes in the cytoplasm. (iii) MNT represses its own transcription in a MAX-dependent manner. (iv) MNT is able to regulate the expression of genes in the absence of MAX. (v) MNT forms homodimers in the cell. Previous reports suggest that MNT functions as a "MYC buffer," curbing excessive MYC activity that would lead to cell transformation. For instance, *in vivo* MNT knockdown antagonizes MYC-driven lymphomagenesis (18, 19), whereas *MNT* silencing leads to MYC-like phenotypes (10, 11, 16). Our data show tight control of MNT expression by which MNT limits its own mRNA expression. These controls suggest that MNT plays a critical function in cell biology. Given the relevance of MNT to modulate MYC activity and its central position between the MYC–MAX and MLX–MONDO networks, the activities and regulation of MNT are key issues for MYC-dependent oncogenesis.

MNT expression was high in some MAX-deficient cells like the rat UR61 cells and human lung carcinoma cell lines deficient in MAX. The absence of MAX was in part responsible for this effect because (i) MAX re-expression in UR61, Lu165, Lu134, and H1417 cells results in decreased MNT protein and mRNA (UR61, H1417, and Lu165), and (ii) MAX overexpression in K562 cells results in MNT down-regulation, whereas MAX knockdown results in MNT up-regulation. The mechanism for this MAX effect on MNT levels depended, at least partially, on the auto-repression of MNT expression by MNT–MAX dimers. Luciferase reporter experiments showed that MNT represses its own promoter (which depends on a conserved E-box), and ChIP assays showed that MNT strongly binds to its own promoter when MAX is ectopically expressed in UR61 cells. MNT binds weaker to its promoter in the absence of MAX, in agreement with a the lack of binding to DNA of MNT *in vitro* (5), and a recent report shows reduced MNT binding to chromatin in MAX-deficient lymphocytes (29). In agreement with these results, the excess levels of MNT localize to the cytoplasm of MAX-deficient cells, whereas MNT is predominantly nuclear in MAX-expressing cells. This would explain why MAX re-expression leads to a decrease in MNT levels; MNT–MAX dimers would be formed to repress MNT expression in the nucleus. On the contrary, in the absence of MAX, MNT is expressed at higher levels because there would be no negative MNT autoregulation. We explored possible MAX-independent effects of MNT using the UR61 model. Although originally MAX was defined as an obligate dimerization partner of MYC, work carried out in the PC12 model and in *Drosophila* indicated that MYC can function in a MAX-independent manner, for example in inhibition of differentiation (30–32). MYC overexpression blocks RAS-induced differentiation of UR61 cells (31), although we did not detect a significant effect of MNT depletion on differentiation (data not shown). In contrast, depletion of MNT in MAX-deficient UR61 cells impairs cell proliferation. To our knowledge, this is the first report on a MAX-independent function of an MXD protein. The fact that MNT depletion impairs UR61 proliferation in a MAX-independent manner adds complexity to the MNT–MYC functional interactions. Conversely to our results in UR61 cells, ablation of *Mnt* in rodent fibroblasts leads to increased proliferation and transformation capacities (10, 16). Actually, in human gastric cancer, high MNT expression correlates with shorter survival, whereas MYC overexpression has the opposite effect (http://kmplot.com/analysis/).[11] Because MNT is a transcription factor, we compared the transcriptomes of parental UR61 cells *versus* cells with depleted MNT. Upon MNT depletion, a number of genes involved in cell cycle progression and DNA damage response were down-regulated in cells with and without MAX. Also, genes involved in cell cycle arrest such as *CDKN1C*/p57 were up-regulated. These gene regulations are concordant with the decrease in proliferation exerted by *MNT* silencing in UR61. It is open to discussion how MNT regulates genes in the absence of MAX. MNT can form heterodimers

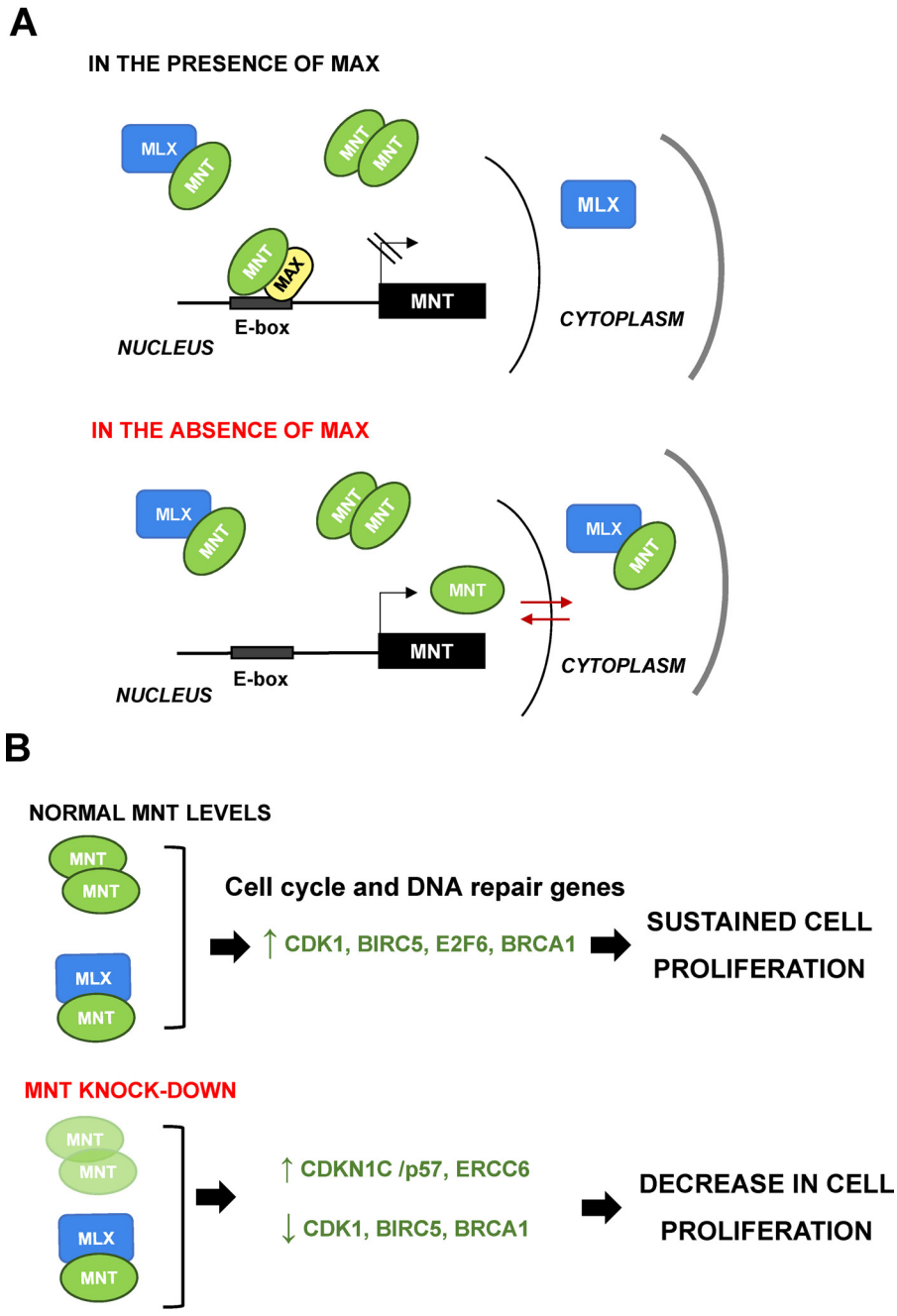

Figure 8. Models of MNT fates and biological roles depending on MAX. *A*, in MAX-expressing cells, most of the MNT is retained in the cell nucleus where it limits its own expression. In MAX-deficient cells as UR61, MNT is distributed in nucleus and cytoplasm and is unable to bind the promoter and regulate its transcriptional activity. The model includes the presence of MNT–MNT homodimers and the interaction MNT–MLX in the cytoplasm, which might be responsible for the MNT partial localization in the cytoplasm in MAX-deficient cells. *B*, model of the biological roles of MNT independent of MAX in UR61 cells. With physiological MNT levels, MNT homodimers and MNT–MLX heterodimers are enhancing cell cycle progression through direct regulation of CDK1 and BIRC5, and DNA repair through BRCA1-dependent mechanisms. However, upon MNT knockdown, this regulation is impaired, with a decrease in CDK1, BIRC5, and BRCA1 and increased levels of CDKN1C, E2F6, and ERCC6. This would cause a cell cycle arrest and the activation of ERCC6-dependent DNA repair mechanisms.

with the HLH protein MLX (6, 27). We have confirmed the ability of MNT to bind MLX in UR61 cells, but when MAX is expressed, the dimers MNT–MAX are favored *versus* MNT–MLX. As a relevant fraction of MLX is cytoplasmic and we have shown that MNT and MLX also interact in the cytoplasm, this interaction could help to explain the increase in cytoplasmic MNT observed in MAX-depleted cells. The model is depicted in Fig. 8*A*.

Moreover, we have shown that MNT homodimerizes in UR61 cells, and therefore it is likely that MNT regulates genes as a homodimer as well. In fact, co-depletion of MLX and MNT does not modify the effect of MNT depletion on genes as *CDKN1C*/p57, *BIRC5*/*Survivin*, *CDK1*, *E2F6*, *BRCA1*, and *PARPB*. Furthermore, ChIP-seq and ChIP–PCR analyses show that MNT binds to some genes in MAX-deficient cells that are regulated by MNT (*BIRC5/Survivin*, *CDK1*, *BRCA1*, *ERCC6*, and *FBXO32*), supporting the possibility of a direct regulation by MNT homodimers or an indirect regulation in other cases where we did not detect MNT binding to the regions assayed (*CDKN1C* and *E2F6*). CDK1 is the only essential CDK protein

for cell cycle progression in animal cells (33). BIRC5/Survivin is also a critical protein for cell survival (34), and we have confirmed its regulation by MNT in URMT cells at the protein level. Thus, the MNT-dependent regulation of both genes helps to explain the antiproliferative effect of MNT knockdown in MAX-deficient cells. Altogether, the data suggest that MNT can regulate transcription as a homodimer or heterodimer with MLX or another not yet identified protein. MNT homodimerization has already been shown in yeast two hybrids (4) and *in vitro* (5), although recombinant MNT homodimers did not bind DNA (5). The analysis of MNT-bound regions in our ChIP-seq experiments also revealed the presence of sites for forkhead factors (FOXP1, FOXA2, and FOXO3) in agreement with the reported coordinated regulation between MNT and FOXO of some cell cycle control genes (25). Further work is required to clarify this point. According to our results, MNT homodimers or MNT–MLX heterodimers would be regulating cell cycle and DNA repair checkpoint genes in a MAX-independent manner for correct survival and proliferation of the cells. The model based on these observations is presented in Fig. 8*B*.

In summary, the results reported here show a strict autoregulation of MNT, supporting a pivotal role of MNT in the control of cell proliferation even in the absence of its canonical dimerization partner MAX.

Experimental procedures

Cell lines and transfections

Cell lines were obtained from ATCC and grown in either RPMI 1640 or Dulbecco's modified Eagle's medium (Lonza) supplemented with 10% fetal bovine serum (Lonza), 150 μg/ml gentamicin, and 2 μg/ml ciprofloxacin. UR61 is derived from PC12 cells (35). All cells tested negative for *Mycoplasma* infection by PCR. To generate the URMT and URMax34 cells, UR61 cells were electroporated (260 V, 1 millifarad, Bio-Rad apparatus) with a pHeBo-MT (to generate URMT cells) or pHeBo-MT–Max vector (to generate URMax34 cells), which carries a human MAX cDNA under the control of metallothionein promoter (24). Cells were selected with 0.2 mg/ml hygromycin (Life Technologies, Inc.), and cell clones were isolated by limiting dilution. Two clones transfected with pHeBo-MT–Max showing MAX induction upon Zn^{2+} addition were pooled, and the resulting cell line was termed URMax34. Five clones transfected with pHeBo-MT were pooled and termed URMT cells. Transient transfections were carried out using the Ingenio electroporation solution (Mirus) in an Amaxa nucleofector. The cells were transfected or transduced with expression vectors for the following: MAX (pCEFL-MAX (36)); MLX β isoform (pMS18-MLX (7)); human MNT (pCMVSport6-MNT, Origene Technologies); MNT–Flag (human MNT with FLAG at the C-terminal lentiviral Lv158 vector, Genecopoeia); MNT–GFP (human MNT with GFP at the N-terminal lentiviral Lv103 vector, Genecopoeia); FL MNT-HA (full-length murine MNT tagged at the C terminus with hemagglutinin epitope (HA)); ΔHLH MNT-HA (murine MNT carrying a deletion of amino acids 221–272 and tagged with HA) (both in pcDNA3 with the Zeocin resistance gene inserted); short-hairpin human MNT-1 (shMNT-1, pLKO-shMNT from Sigma Mission, TRCN0000085733) or MNT-2 (shMNT-2, pLKO-shMNT from Sigma Mission, TRCN0000235815); siRNA for human MAX (Sigma, SASI_Hs01_00011941).

Immunoblot and immunoprecipitation

Cell lysis, immunoblots, and immunoprecipitations were performed as described (37). Each immunoblot shows a representative experiment out of at least two biological replicates with similar results. The antibodies used are described in Table S7.

Luciferase reporters and assays

To generate the MNT-luc, E-box 1 MNT-luc, and E-box 2 MNT-luc reporter vectors, two pairs of primers were designed for each construct (Table S8), targeting sequences of the human genome corresponding to 850 bp upstream from the transcription start site of the *MNT* gene. The amplified DNA was inserted into the pBV-luc reporter vector at the EcoRV and HindIII sites (38). The sequence of the MNT promoter was from the UCSC genome browser. Cells were transfected with jetPEI® reagent (Polyplus), and luciferase assays were performed, as described previously (37).

Cell proliferation, cell cycle, and annexin V–binding analysis

Cell proliferation was monitored with a cell counter (NucleoCounter NC-100, Chemometec) or a cytometer (Guava PCA, Merck Millipore). For the clonogenic assays, $1–2 \times 10^6$ cells/ml were seeded in a 6-well or 60-mm plate after transfection by electroporation. 48 h post-transfection, cells were selected with puromycin at 0.2–0.5 μg/ml final concentration. After 8–17 days, the cells were stained with crystal violet, and the dye was measured by absorbance at 595 nm as described (39). To determine the sub-G_0–G_1 population, cells were transfected, and 7 days post-transfection, the DNA concentration was analyzed by propidium iodide staining and flow cytometry as described (40). Apoptosis was assayed by annexin V–positive binding in MACSQuant VYB (Miltenyi Biotec). Roughly, 10^6 cells were harvested and washed twice with previously filtered PBS and 3 mM EDTA. Cells were resuspended in 10 mM HEPES/NaOH, pH 7.4, and stained with 5 μl of annexin V–FITC (BD Biosciences) for 1 h. Cells were washed twice and resuspended in 500 μl of binding buffer with 5 μl of 7-aminoactinomycin D (Immunostep apoptosis detection kit). The results were analyzed with Flow Logic software (Miltenyi Biotec).

RNA analysis and RNA-seq

For qPCR, total RNA was isolated using the TRI Reagent Solution (Invitrogen). cDNA was generated by reverse transcription (RT) using the iScript (Bio-Rad). Quantitative PCR (qPCR) was performed with specific primers (Table S8) using the iTaq Universal SYBR Green Supermix (Bio-Rad) and CFX Connect Real-Time PCR Detection System (Bio-Rad). RNA was converted into cDNA and analyzed as described (41). Levels of mRNA were normalized against actin and RPS14 mRNA levels. For RNA-seq , total RNA was isolated with the RNeasy kit (Qiagen) from two independent experiments of MNT silencing in URMT and URMax34 cells, both treated with 100

μM $ZnSO_4$ for 24 h. mRNA libraries were prepared using the Illumina TruSeq RNA Sample Prep kit version 2 (kit RS-122-2002, Illumina). A minimum of 40 million 50-base single-end reads per sample were obtained. TopHat algorithm (42) was used to align the data using a set of gene model annotations and/or known transcripts of rat genome obtained from RefSeq database. Cufflinks software (43) was run to estimate transcript abundances represented in RPKM units (reads per kilobase per million reads) as described (44). The gene expression of the genes are represented as RPKM values. The log2 RPKM values of the transcripts that were differentially expressed in URMT and URMax34 cells were represented in a dot graph with the log2 RPKM values of the control condition (pLKO) on the *x* axis and the log2 RPKM values of the experimental condition (shMNT) on the *y* axis.

ChIP and ChIP-seq

Total-cell extracts were first lysed with a hypotonic buffer (described under "Nuclear/cytoplasmic fractionation") for purifying the nuclear compartment. Then, nuclear lysis and ChIP were performed essentially as described previously (37). Immunoprecipitated DNA was purified with the QIAquick PCR purification kit (Qiagen) and analyzed by qPCR. The antibodies and primers used are described in Tables S7 and S8, respectively. For ChIP–PCR, chromatin was prepared from URMT and URMax34 cells (both treated with 100 μM $ZnSO_4$ for 24 h) and immunoprecipitated with anti-MNT antibody and unspecific IgG. For ChIP-seq, we used MNT-bound chromatin and the corresponding inputs from URMT cells. Single-end 51-bp ChIP-seq data from three replicate experiments and three input samples of URMT cells were generated by HiSeq. Alignment and peak detection were performed using the ENCODE (phase-3) transcription factor ChIP-seq pipeline specifications (45). Reads were aligned to the rat reference genome (assembly Rnor_6.0) using BWA (46), removing duplicates with PICARD (Picard Toolkit 2018, http://broadinstitute.github.io/picard)[11] and filtering all reads with a quality score <30. Peaks were called using SPP (47) and input samples as background samples. Enrichment and quality measures were computed with Phantompeakqualtools (48). Reproducibility of peaks identified from the three replicate experiments was measured using IDR with a threshold of 0.1. Peak annotation was performed with Homer (http://homer.ucsd.edu/homer/motif/motifDatabase.html)[11] (49).

The SYDH ENCODE project was chosen for representation of the binding peaks in the promoter of the human MNT gene. The sequences corresponding to those peaks were analyzed confirming the presence of the E-boxes identified in the human MNT promoter. Enriched motifs on immunoprecipitated regions were identified by HOMER (49) FindMotifsGenome algorithm using the rat genome Rnor_6.0 version as reference, masking common repeats and with a region size of 200 bp (http://homer.ucsd.edu/homer/motif/motifDatabase.html).[11] The RNA-seq and ChIP-seq data have been deposited to the European Nucleotide Archive with the accession number PRJEB23604.

Nuclear/cytoplasmic fractionation

Cytoplasmic and nuclear extracts were prepared essentially as described (50). The hypotonic buffer to lyse cells was 10 mM HEPES, pH 7, 10 mM KCl, 0.25 mM EDTA, pH 8, 0.125 mM EGTA, pH 8, 0.5 mM spermidine, 0.1% Nonidet P-40, 1 mM DTT, and proteases inhibitors. The hypertonic buffer for nuclear extracts was 20 mM HEPES, 400 mM NaCl, 0.25 mM EDTA, 1.5 mM $MgCl_2$, 0.5 mM DTT, and proteases inhibitors.

Statistical analysis

Student's *t* test was used to evaluate the significance of differences between control and experimental groups. A *p* value of less than 0.05 was considered as significant. The threshold for expression changes in the RNA-seq analysis was set as log2(RPKM fold change) ≥ 0.7 or ≤ -0.7 and a *p* value <0.1.

Author contributions—M. C. L.-N., J. L.-P., O. A. R., M. S.-C., R. N. E., and M. D. D. formal analysis; M. C. L.-N., J. L.-P., A. Q., I. V., R. B., F. O., G. B., J. A., E. M., P. C., P. H., and O. A. R. investigation; M. C. L.-N., J. L.-P., A. Q., R. B., and J. A. methodology; M. C. L.-N., J. L.-P., I. V., R. N. E., M. D. D., and J. L. writing-review and editing; I. V. data curation; I. V. software; P. C., P. H., O. A. R., M. S.-C., R. N. E., M. D. D., and J. L. resources; R. N. E. and J. L. funding acquisition; J. L. conceptualization; J. L. supervision; J. L. writing-original draft.

Acknowledgments—We are grateful to Don Ayer for cell lines and constructs, Maralice Conacci-Sorrel for comments on the manuscript, and Sandra Zunzunegui and Maria Aramburu for technical help. We also thank Dreamgenics (Oviedo, Spain) for their help in ChIP analysis.

References

1. Schaub, F. X., Dhankani, V., Berger, A. C., Trivedi, M., Richardson, A. B., Shaw, R., Zhao, W., Zhang, X., Ventura, A., Liu, Y., Ayer, D. E., Hurlin, P. J., Cherniack, A. D., Eisenman, R. N., Bernard, B., *et al.* (2018) Pan-cancer alterations of the MYC oncogene and its proximal network across the cancer genome atlas. *Cell Syst.* **6,** 282–300.e2 CrossRef Medline
2. Dang, C. V. (2012) MYC on the path to cancer. *Cell* **149,** 22–35 CrossRef Medline
3. Conacci-Sorrell, M., McFerrin, L., and Eisenman, R. N. (2014) An overview of MYC and its interactome. *Cold Spring Harb. Perspect. Med.* **4,** a014357 CrossRef Medline
4. Meroni, G., Reymond, A., Alcalay, M., Borsani, G., Tanigami, A., Tonlorenzi, R., Lo Nigro, C., Messali, S., Zollo, M., Ledbetter, D. H., Brent, R., Ballabio, A., and Carrozzo, R. (1997) Rox, a novel bHLHZip protein expressed in quiescent cells that heterodimerizes with Max, binds a non-canonical E box and acts as a transcriptional repressor. *EMBO J.* **16,** 2892–2906 CrossRef Medline
5. Hurlin, P. J., Qúeva, C., and Eisenman, R. N. (1997) Mnt: a novel Max-interacting protein and Myc antagonist. *Curr. Top. Microbiol. Immunol.* **224,** 115–121 CrossRef Medline
6. Meroni, G., Cairo, S., Merla, G., Messali, S., Brent, R., Ballabio, A., and Reymond, A. (2000) Mlx, a new Max-like bHLHZip family member: the center stage of a novel transcription factors regulatory pathway? *Oncogene* **19,** 3266–3277 CrossRef Medline
7. Billin, A. N., Eilers, A. L., Queva, C., and Ayer, D. E. (1999) Mlx, a novel Max-like BHLHZip protein that interacts with the Max network of transcription factors. *J. Biol. Chem.* **274,** 36344–36350 CrossRef Medline
8. Yang, G., and Hurlin, P. J. (2017) MNT and emerging concepts of MNT–MYC antagonism. *Genes* **8,** E83 CrossRef Medline
9. Diolaiti, D., McFerrin, L., Carroll, P. A., and Eisenman, R. N. (2015) Functional interactions among members of the MAX and MLX transcriptional

network during oncogenesis. *Biochim. Biophys. Acta* **1849,** 484–500 CrossRef Medline
10. Hurlin, P. J., Zhou, Z. Q., Toyo-oka, K., Ota, S., Walker, W. L., Hirotsune, S., and Wynshaw-Boris, A. (2003) Deletion of Mnt leads to disrupted cell cycle control and tumorigenesis. *EMBO J.* **22,** 4584–4596 CrossRef Medline
11. Walker, W., Zhou, Z. Q., Ota, S., Wynshaw-Boris, A., and Hurlin, P. J. (2005) Mnt–Max to Myc–Max complex switching regulates cell cycle entry. *J. Cell Biol.* **169,** 405–413 CrossRef Medline
12. Toyo-oka, K, Hirotsune, S., Gambello, M. J., Zhou, Z. Q., Olson, L., Rosenfeld, M. G., Eisenman, R., Hurlin, P., and Wynshaw-Boris, A. (2004) Loss of the Max-interacting protein Mnt in mice results in decreased viability, defective embryonic growth and craniofacial defects: relevance to Miller-Dieker syndrome. *Hum. Mol. Genet.* **13,** 1057–1067 CrossRef Medline
13. Foley, K. P., McArthur, G. A., Quéva, C., Hurlin, P. J., Soriano, P., and Eisenman, R. N. (1998) Targeted disruption of the MYC antagonist MAD1 inhibits cell cycle exit during granulocyte differentiation. *EMBO J.* **17,** 774–785 CrossRef Medline
14. Quéva, C., McArthur, G. A., Ramos, L. S., and Eisenman, R. N. (1999) Dwarfism and dysregulated proliferation in mice overexpressing the MYC antagonist MAD1. *Cell Growth Differ.* **10,** 785–796 Medline
15. Schreiber-Agus, N., and DePinho, R. A. (1998) Repression by the Mad(Mxi1)–Sin3 complex. *Bioessays* **20,** 808–818 CrossRef Medline
16. Nilsson, J. A., Maclean, K. H., Keller, U. B., Pendeville, H., Baudino, T. A., and Cleveland, J. L. (2004) Mnt loss triggers Myc transcription targets, proliferation, apoptosis, and transformation. *Mol. Cell. Biol.* **24,** 1560–1569 CrossRef Medline
17. Dezfouli, S., Bakke, A., Huang, J., Wynshaw-Boris, A., and Hurlin, P. J. (2006) Inflammatory disease and lymphomagenesis caused by deletion of the Myc antagonist Mnt in T cells. *Mol. Cell. Biol.* **26,** 2080–2092 CrossRef Medline
18. Link, J. M., Ota, S., Zhou, Z. Q., Daniel, C. J., Sears, R. C., and Hurlin, P. J. (2012) A critical role for Mnt in Myc-driven T-cell proliferation and oncogenesis. *Proc. Natl. Acad. Sci. U.S.A.* **109,** 19685–19690 CrossRef Medline
19. Campbell, K. J., Vandenberg, C. J., Anstee, N. S., Hurlin, P. J., and Cory, S. (2017) Mnt modulates Myc-driven lymphomagenesis. *Cell Death Differ.* **24,** 2117–2126 CrossRef Medline
20. Hopewell, R., and Ziff, E. B. (1995) The nerve growth factor-responsive PC12 cell line does not express the Myc dimerization partner Max. *Mol. Cell. Biol.* **15,** 3470–3478 CrossRef Medline
21. Romero, O. A., Torres-Diz, M., Pros, E., Savola, S., Gomez, A., Moran, S., Saez, C., Iwakawa, R., Villanueva, A., Montuenga, L. M., Kohno, T., Yokota, J., and Sanchez-Cespedes, M. (2014) MAX inactivation in small-cell lung cancer disrupts MYC-SWI/SNF programs and is synthetic lethal with BRG1. *Cancer Discov.* **4,** 292–303 CrossRef Medline
22. Popov, N., Wahlström, T., Hurlin, P. J., and Henriksson, M. (2005) Mnt transcriptional repressor is functionally regulated during cell cycle progression. *Oncogene* **24,** 8326–8337 CrossRef Medline
23. Blackwood, E. M., Kretzner, L., and Eisenman, R. N. (1992) Myc and Max function as a nucleoprotein complex. *Curr. Opin. Genet. Dev.* **2,** 227–235 CrossRef Medline
24. Cañelles, M., Delgado, M. D., Hyland, K. M., Lerga, A., Richard, C., Dang, C. V., and León, J. (1997) Max and inhibitory c-Myc mutants induce erythroid differentiation and resistance to apoptosis in human myeloid leukemia cells. *Oncogene* **14,** 1315–1327 CrossRef Medline
25. Terragni, J., Nayak, G., Banerjee, S., Medrano, J. L., Graham, J. R., Brennan, J. F., Sepulveda, S., and Cooper, G. M. (2011) The E-box binding factors Max/Mnt, MITF, and USF1 act coordinately with FoxO to regulate expression of proapoptotic and cell cycle control genes by phosphatidylinositol 3-kinase/Akt/glycogen synthase kinase 3 signaling. *J. Biol. Chem.* **286,** 36215–36227 CrossRef Medline
26. Lafita-Navarro, M. C., Blanco, R., Mata-Garrido, J., Liaño-Pons, J., Tapia, O., Garcia-Gutiérrez, L., García-Alegría, E., Berciano, M. T., Lafarga, M., and León, J. (2016) MXD1 localizes in the nucleolus, binds UBF and impairs rRNA synthesis. *Oncotarget* **7,** 69536–69548 CrossRef Medline
27. Cairo, S., Merla, G., Urbinati, F., Ballabio, A., and Reymond, A. (2001) WBSCR14, a gene mapping to the Williams–Beuren syndrome deleted region, is a new member of the Mlx transcription factor network. *Hum. Mol. Genet.* **10,** 617–627 CrossRef Medline
28. Billin, A. N., Eilers, A. L., Coulter, K. L., Logan, J. S., and Ayer, D. E. (2000) MondoA, a novel basic helix-loop-helix-leucine zipper transcriptional activator that constitutes a positive branch of a max-like network. *Mol. Cell. Biol.* **20,** 8845–8854 CrossRef Medline
29. Mathsyaraja, H., Freie, B., Cheng, P. F., Babaeva, E., Catchpole, J. T., Janssens, D., Henikoff, S., and Eisenman, R. N. (2019) Max deletion destabilizes MYC protein and abrogates Emicro-Myc lymphomagenesis. *Genes Dev.* **33,** 1252–1264 CrossRef Medline
30. Maruyama, K., Schiavi, S. C., Huse, W., Johnson, G. L., and Ruley, H. E. (1987) myc and E1A oncogenes alter the responses of PC12 cells to nerve growth factor and block differentiation. *Oncogene* **1,** 361–367 Medline
31. Vaqué, J. P., Fernández-García, B., García-Sanz, P., Ferrandiz, N., Bretones, G., Calvo, F., Crespo, P., Marín, M. C., and León, J. (2008) c-Myc inhibits Ras-mediated differentiation of pheochromocytoma cells by blocking c-Jun up-regulation. *Mol. Cancer Res.* **6,** 325–339 CrossRef Medline
32. Gallant, P. (2013) Myc function in *Drosophila*. *Cold Spring Harb. Perspect. Med.* **3,** a014324 CrossRef Medline
33. Santamaría, D., Barrière, C., Cerqueira, A., Hunt, S., Tardy, C., Newton, K., Cáceres, J. F., Dubus, P., Malumbres, M., and Barbacid, M. (2007) Cdk1 is sufficient to drive the mammalian cell cycle. *Nature* **448,** 811–815 CrossRef Medline
34. Altieri, D. C. (2015) Survivin- The inconvenient IAP. *Semin. Cell Dev. Biol.* **39,** 91–96 CrossRef Medline
35. Guerrero, I., Pellicer, A., and Burstein, D. E. (1988) Dissociation of c-fos from ODC expression and neuronal differentiation in a PC12 subline stably transfected with an inducible N-ras oncogene. *Biochem. Biophys. Res. Commun.* **150,** 1185–1192 CrossRef Medline
36. Mauleon, I., Lombard, M. N., Muñoz-Alonso, M. J., Cañelles, M., and Leon, J. (2004) Kinetics of myc-max-mad gene expression during hepatocyte proliferation *in vivo*: Differential regulation of mad family and stress-mediated induction of c-myc. *Mol. Carcinog.* **39,** 85–90 CrossRef Medline
37. Garcia-Sanz, P., Quintanilla, A., Lafita, M. C., Moreno-Bueno, G., García-Gutierrez, L., Tabor, V., Varela, I., Shiio, Y., Larsson, L. G., Portillo, F., and Leon, J. (2014) Sin3b interacts with myc and decreases myc levels. *J. Biol. Chem.* **289,** 22221–22236 CrossRef Medline
38. He, T. C., Sparks, A. B., Rago, C., Hermeking, H., Zawel, L., da Costa, L. T., Morin, P. J., Vogelstein, B., and Kinzler, K. W. (1998) Identification of c-MYC as a target of the APC pathway. *Science* **281,** 1509–1512 CrossRef Medline
39. Ferrandiz, N., Martin-Perez, J., Blanco, R., Donertas, D., Weber, A., Eilers, M., Dotto, P., Delgado, M. D., and Leon, J. (2009) HCT116 cells deficient in p21(Waf1) are hypersensitive to tyrosine kinase inhibitors and adriamycin through a mechanism unrelated to p21 and dependent on p53. *DNA Repair* **8,** 390–399 CrossRef Medline
40. Albajar, M., Gómez-Casares, M. T., Llorca, J., Mauleon, I., Vaqué, J. P., Acosta, J. C., Bermúdez, A., Donato, N., Delgado, M. D., and León, J. (2011) MYC in chronic myeloid leukemia: induction of aberrant DNA synthesis and association with poor response to imatinib. *Mol. Cancer Res.* **9,** 564–576 CrossRef Medline
41. Bretones, G., Acosta, J. C., Caraballo, J. M., Ferrándiz, N., Gómez-Casares, M. T., Albajar, M., Blanco, R., Ruiz, P., Hung, W. C., Albero, M. P., Perez-Roger, I., and León, J. (2011) SKP2 oncogene is a direct MYC target gene and MYC down-regulates p27(KIP1) through SKP2 in human leukemia cells. *J. Biol. Chem.* **286,** 9815–9825 CrossRef Medline
42. Trapnell, C., Pachter, L., and Salzberg, S. L. (2009) TopHat: discovering splice junctions with RNA-seq . *Bioinformatics* **25,** 1105–1111 CrossRef Medline
43. Trapnell, C., Williams, B. A., Pertea, G., Mortazavi, A., Kwan, G., van Baren, M. J., Salzberg, S. L., Wold, B. J., and Pachter, L. (2010) Transcript assembly and quantification by RNA-seq reveals unannotated transcripts and isoform switching during cell differentiation. *Nat. Biotechnol.* **28,** 511–515 CrossRef Medline
44. Mortazavi, A., Williams, B. A., McCue, K., Schaeffer, L., and Wold, B. (2008) Mapping and quantifying mammalian transcriptomes by RNA-seq. *Nat. Methods* **5,** 621–628 CrossRef Medline

45. ENCODE Project Consortium. (2012) An integrated encyclopedia of DNA elements in the human genome. *Nature* **489,** 57–74 CrossRef Medline
46. Li, H., and Durbin, R. (2009) Fast and accurate short read alignment with Burrows-Wheeler transform. *Bioinformatics* **25,** 1754–1760 CrossRef Medline
47. Kharchenko, P. V., Tolstorukov, M. Y., and Park, P. J. (2008) Design and analysis of ChIP-seq experiments for DNA-binding proteins. *Nat. Biotechnol.* **26,** 1351–1359 CrossRef Medline
48. Landt, S. G., Marinov, G. K., Kundaje, A., Kheradpour, P., Pauli, F., Batzoglou, S., Bernstein, B. E., Bickel, P., Brown, J. B., Cayting, P., Chen, Y., DeSalvo, G., Epstein, C., Fisher-Aylor, K. I., Euskirchen, G., *et al.* (2012) ChIP-seq guidelines and practices of the ENCODE and modENCODE consortia. *Genome Res.* **22,** 1813–1831 CrossRef Medline
49. Heinz, S., Benner, C., Spann, N., Bertolino, E., Lin, Y. C., Laslo, P., Cheng, J. X., Murre, C., Singh, H., and Glass, C. K. (2010) Simple combinations of lineage-determining transcription factors prime cis-regulatory elements required for macrophage and B cell identities. *Mol. Cell* **38,** 576–589 CrossRef Medline
50. Conacci-Sorrell, M., Ngouenet, C., and Eisenman, R. N. (2010) Myc-nick: a cytoplasmic cleavage product of Myc that promotes α-tubulin acetylation and cell differentiation. *Cell* **142,** 480–493 CrossRef Medline